D R A F T - 2A

A Letter of Intent to the Jefferson Lab PAC43

Search for Gluonic Excitations of Light Quark Baryons with CLAS12 and the Forward Tagger in Hall B

A. D'Angelo,[1,2] V. Burkert,[3] S. Capstick,[4] G. Fedotov,[9] E. Golovach,[5] R. Gothe,[6] B.S. Ishkhanov,[5,9] L. Lanza,[2] V. Mokeev,[3] A. Rizzo,[2] J. Ryckebusch,[7] Iu. Skorodumina,[9] A. Szczepaniak,[8,3] M. Ungaro,[3] and V. Ziegler[3]

[1] *INFN, Sezione di Roma Tor Vergata, 00133 Rome, Italy*
[2] *Universita' di Roma Tor Vergata, 00133 Rome Italy*
[3] *Thomas Jefferson National Accelerator Facility, Newport News, Virginia 23606, USA*
[4] *Florida State University, Tallahassee, Florida 32306, USA*
[5] *Skobeltsyn Institute of Nuclear Physics, Lomonosov Moscow State University, 119234 Moscow, Russia*
[6] *University of South Carolina, Columbia, South Carolina 29208, USA*
[7] *Gent University, Gent, Netherland*
[8] *Indiana University, Nuclear Theory Center, Bloomington, Indiana*
[9] *Physics Department at Lomonosov Moscow State University, Leninskie Gory, Moscow 119991, Russia.*

(Dated: April 23, 2015)

We intent to submit a proposal to an upcoming Jefferson Lab program Advisory Committee to launch an experimental program that will utilize the CLAS12 detector system in Hall B augmented by the Forward Tagger (FT) with the goal of studying the s-channel excitation of baryons with dominant gluonic excitation strength (hybrid baryons). The experiment will use electron beams with energies of 6.6, 8.8 and 11 GeV impinging on a liquid hydrogen target in the CLAS12 center. Scattered electrons will be detected in an angle range of 2.5 to 4.5 degrees by detecting electromagnetic energy in the electromagnetic calorimeter that is part of the Forward Tagger covering a Q^2 range of 0.05 0.5 GeV^2. Electrons scattered at polar angles greater than 6 -7 degrees will be detected and reconstructed in the CLAS12 detector system using the High Threshold Cherenkov Counter (HTCC) and the sequence of pre-shower calorimeter (PCAL) and the electromagnetic calorimeter (EC). The virtual exchange photons will be linearly polarized. At the requested beam energies, the mass range $W < 3.5$ GeV will be covered. Due to the high electron rate at the very forward polar angles, additional constraints on the hadronic final state will be built into the CLAS12 trigger system to reduce the recorded event rate to a maximum of 20KHz.

Contents

I. INTRODUCTION

The ongoing program at Jefferson Lab and several other laboratories to study the excitation of nucleons in the so-called nucleon resonance region with real photon and with electron beams has been very successful. Although only a fraction of the data taken during the CLAS run groups g8, g9, g10, and g12 have been analyzed and published, the published data have allowed to make very significant advances in light-quark baryon spectroscopy, and led to strong evidence of several new nucleon excitations as listed in the PDG listing of 2014 [1]. These discoveries were possible due to the very high meson production rates possible in the energy-tagged photoproduction processes. Furthermore, the use of meson electroproduction has led to completely new insights into the nature of several prominent resonant baryons, e.g. the so-called Roper resonance $N(1440)\frac{1}{2}^+$. This state defied an explanation of its properties, such as mass, transition amplitudes and transition form factors within the constituent quark model (CQM). The analyses of the new electroproduction data was crucial in dissecting its complex structure and providing a qualitative and quantitative explanation of the space-time evolution of the state [2]. For example, the Roper was considered as a candidate for the lowest mass hybrid baryon [3]. It was only through the meson electroproduction data that this possibility could be dismissed [4, 5].

The theory of the strong interactions, QCD, not only allows for the existence of hybrid baryons, but Lattice QCD calculations now predict several baryon states with strong gluonic content, with the lowest mass hybrids approximately 1.3 GeV above the nucleon ground state of 0.94 GeV, i.e. in the range $W = 2.2 - 2.3$ GeV. In the meson sector, exotic states (hybrid mesons) are predicted with quantum numbers that cannot be obtained in pure $q\bar{q}$ configuration. The selection of mesons with such exotic quantum numbers provides a convenient way to identify candidates for gluonic mesons. In contrast to the meson sector gluonic baryons (hybrid baryons) have quantum numbers that are also populated by ordinary excited 3-quark states. Hybrid baryons can mix with ordinary 3-quark excited states or with dynamically generated states making the identification of gluonic baryons more difficult. An important question is therefore: How can we distinguish gluonic excitations of baryons from their ordinary quark excitations? Another question is the mass range in which we may expect hybrid baryons to occur.

Mapping out the nucleon spectrum and the excitation strengths of individual resonances is a powerful way to answer a central question of hadron physics: "What are the effective degrees of freedom as the excited states are probed at different distance scales?". Previous analyses of meson electroproduction have shown to be most effective in providing answers in several cases of excited states: $\Delta(1232)\frac{3}{2}^+$, $N(1440)\frac{1}{2}^+$, $N(1520)\frac{3}{2}^-$, $N(1535)\frac{1}{2}^-$, $N(1680)\frac{5}{2}^+$, $N(1675)\frac{5}{2}^-$. The experimental program outlined in this Letter-of-Intent is meant to vastly improve upon the available information and extend the reach of meson electroproduction to cover the full nucleon resonance mass range up to over 3.5GeV and a larger Q^2 range. In conjunction with experiment E12-09-003, which focusses on the highest Q^2, the proposed experiment will provide a complete program of nucleon resonance electroexcitation.

II. THEORETICAL STUDIES

A. Model projections

Gluonic excitations of the nucleon have been broadly discussed first in 1983 [3] in an extension of the MIT bag model to states where a constituent gluon in the lowest energy transverse electric mode combines with three quarks in a color octet state to form a colorless state in the mass range of 1.600 ± 0.100 GeV [4]. The glue flux-tube model applied to hybrid baryons [6, 7] came up with similar quantum numbers of the hybrid states, but predicted considerably higher masses than the bag model. For the lowest mass hybrid baryon a mass of 1.870 ± 0.100 GeV was found. In all cases the lowest mass hybrid baryon was predicted as a $J^P = 1/2^+$ state, i.e. a nucleon-like or Roper-like state. Hybrid baryons were also discussed in the Large N_c approximation of QCD for heavy quarks [8], which also led to the justification of the constituent glue picture used in the models. The high energy behavior of hybrid baryons was discussed in [9]. However, in contrast to hybrid meson production, which has received great attention both in theory and in experiments, the perceived difficulties of isolating hybrid baryon states from ordinary quark states let this part of the field to remain dormant for a decade.

B. Lattice QCD predictions

The first quenched calculations on the lattice came in 2003 [10], where the lowest gluonic excitation of the 3-quark system was projected at a mass of 1 GeV above the nucleon mass, placing the lowest hybrid baryon at a mass around 2 GeV. The first LQCD calculation of the full light-quark baryon spectrum with unquenched quarks occurred in

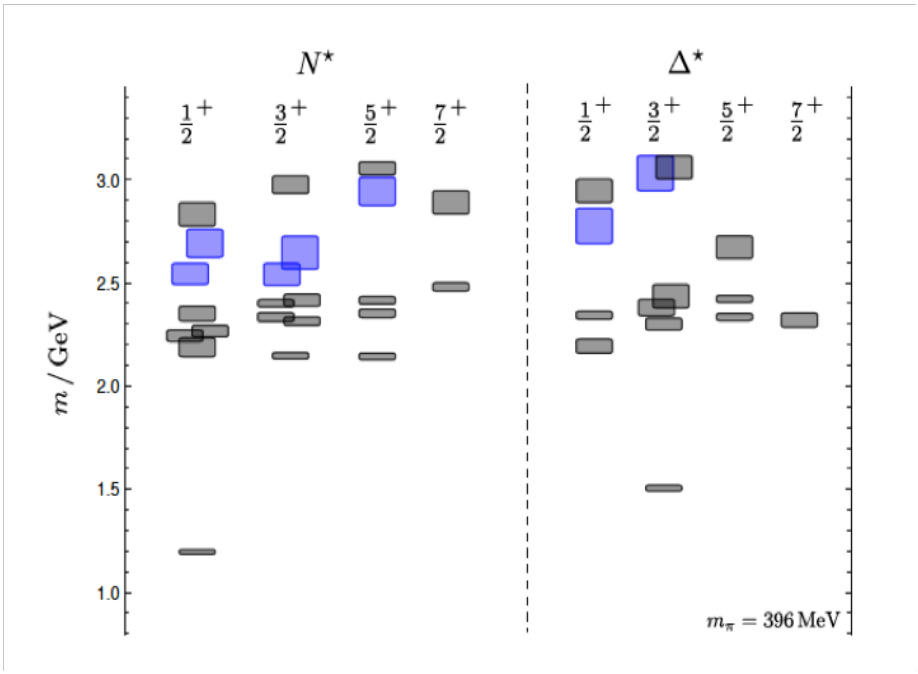

FIG. 1: The light-quark baryon spectrum predicted in Lattice QCD at a pion mass of 396 MeV. The blue shaded boxes indicate states with dominant gluonic excitations. Note that both the mass of the nucleon ground state and of the $\Delta(1232)$ are shifted by nearly 300 MeV to higher masses. This is largely due to the pion mass of 396MeV.

2012 that included the projections of the hybrid nucleon N_G states and hybrid Δ_G states [11]. Figure 1 shows the projected light quark baryon spectrum in the lower mass range. At the pion mass of 396 MeV used in this projection, the prediction for the lowest hybrid nucleon $J^P = \frac{1}{2}^+$ state, gives a mass of about 1.3 GeV above the nucleon ground state, i.e. in a mass range of 2.2 - 2.3 GeV (note that in this calculation the nucleon mass is shifted by nearly 300 MeV to higher masses). In the following we take this shift into account by subtracting 300 MeV from the masses of excited states in Fig. 1. As stated in [11], the lowest hybrid baryons, shown in Fig. 1 in blue, were identified as states with leading gluonic excitations. If hybrid baryons are not too wide, we might expect the lowest hybrid baryon to occur in a mass range of 2.2 - 2.3 GeV, a few hundred MeV above the band of radially excited $J^P = \frac{1}{2}^+$ 3-quark nucleon excitations of isospin $\frac{1}{2}$ and thus possibly well separated from other states. In this computation the lowest $J^P = \frac{3}{2}^+$ gluonic states are nearly mass degenerate with the corresponding $J^P = \frac{1}{2}^+$ gluonic states generating a glue-rich mass range of hybrid nucleons. If these projections hold up with LQCD calculations using near physical pion masses, one should expect a band of the lowest mass hybrid baryon states with spin-parity $\frac{1}{2}^+$ and $\frac{3}{2}^+$ to populate a relatively narrow mass band of $2.2 - 2.5$ GeV. Note, that these states fall into a mass range where no excited quark nucleon states are predicted to exist from these calculations. The corresponding negative parity hybrid states are expected to occur at much higher masses and are not included in this graph, and are not further considered here, although they may be subject of analysis should they appear within the kinematics covered by this LoI.

C. Hadronic couplings

Very little is known about possible hadronic couplings of hybrid baryons. One might expect an important role for final states with significant gluonic content, e.g. $B_G \to N\eta'$, or final states containing $s\bar{s}$ contributions due to the coupling $G \to s\bar{s}$, e.g. $B_G \to K^+\Lambda$, $B_G \to N^*(1535)\pi \to N\eta\pi$, $B_G \to N\pi\pi$, $B_G \to \phi(1020)N$ and $B_G \to K^*\Lambda$. Quark-model estimates of the hadronic couplings would be helpful in selecting the most promising final state for the experimental evaluation. As long as such estimates are not available we will use a range of assumptions on the hadronic couplings to estimate the sensitivity required for definitive measurements. Assuming hadronic couplings of a few % in the less complex final states, e.g. $K^+\Lambda$, $K^*\Lambda$, or $N\pi\pi$ we should be able to identify these estates and

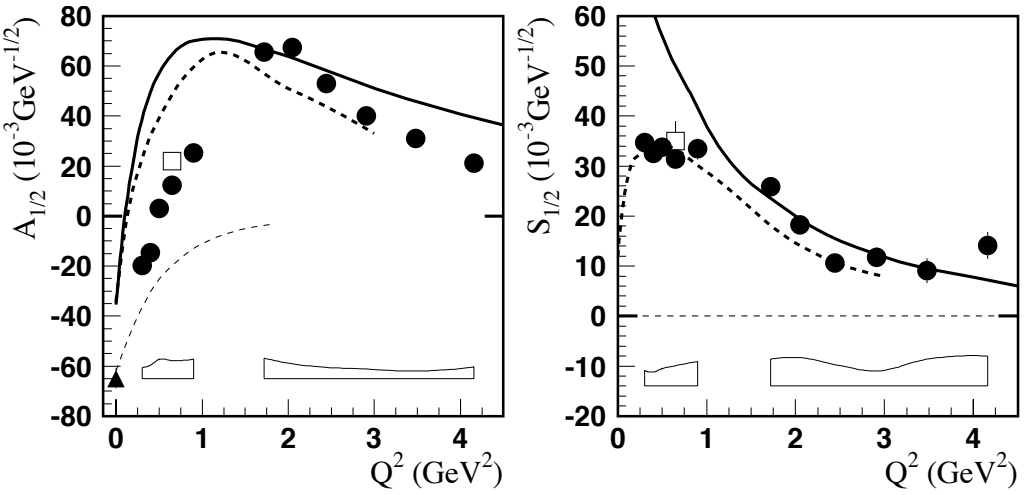

FIG. 2: Electrocoupling amplitudes of the Roper resonance $N(1440)\frac{1}{2}^+$. The thin dashed lines are the constituent quark-glue model predictions for the gluonic Roper.

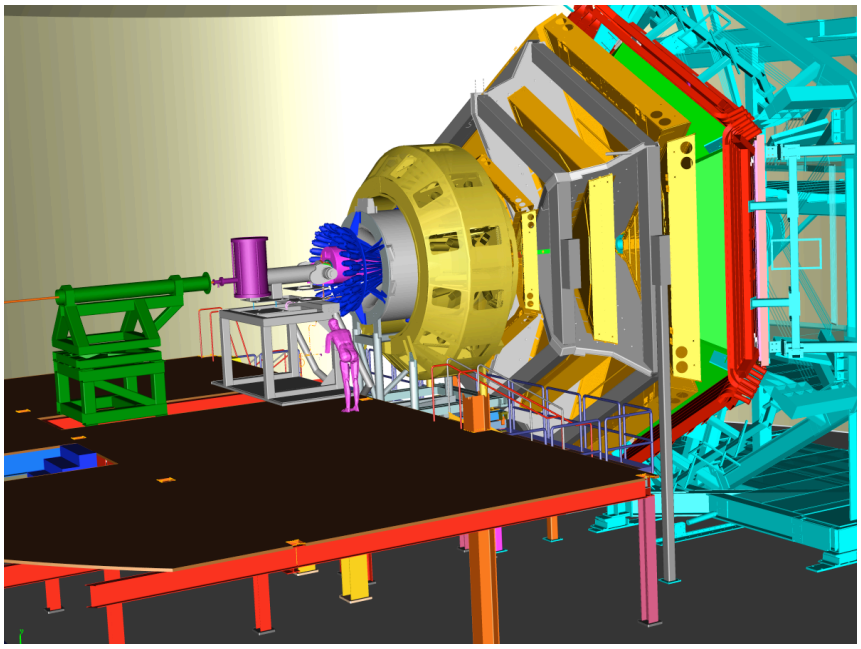

FIG. 3: The CLAS12 detector.

proceed to establish their electromagnetic couplings and Q^2 dependance.

D. Electromagnetic couplings

Electromagnetic couplings have been studied within a non-relativistic constituent quark-gluon model and only for two possible hybrid states, the Roper $N_G(1440)\frac{1}{2}^+$ and the $\Delta_G(1600)\frac{3}{2}^+$. In reference [13] the photoexcitation of the hybrid Roper resonance $N(1440)\frac{1}{2}^+$ was studied, and in reference [14] the electroproduction transition form factors of

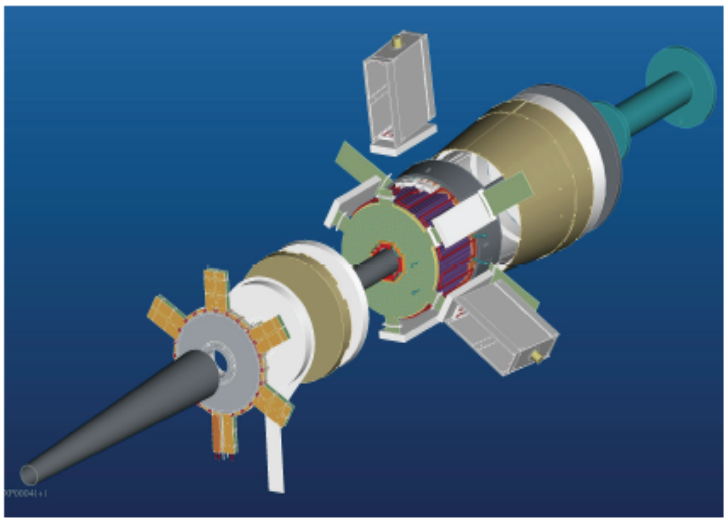

FIG. 4: The Forward Tagger (FT) system. The FT provides electron and high energy photon detection in a range of polar angles $\theta_e = 2.5^\circ - 4.5^\circ$, and will be fully integrated into the operation of CLAS12. Details on the specifications and expected operational performance may be obtained from https://www.jlab.org/Hall-B/clas12-web/specs/ft.pdf.

a hybrid Roper state were evaluated. The latter was essential in eliminating the Roper resonance as a candidate for a hybrid state, both due to the transverse helicity amplitude and its Q^2 dependence and the prediction of $S_{1/2}(Q^2) = 0$ at all Q^2. It also showed that a hybrid Roper transition amplitudes should behave like the ones of the ordinary $\Delta(1232)\frac{3}{2}^+$ for both its transition amplitudes. Recent measurements of the electrocoupling transition amplitudes are shown in Figure 2. Both amplitudes exhibit a Q^2 dependence that is distinctively different from the gluonic baryon prediction. Especially the scalar amplitude $S_{1/2}(Q^2)$ was found to be large while it is predicted to be equal zero in leading order.

The aforementioned predictions should apply to the lowest mass hybrid state with $J^P = \frac{1}{2}^+$. One may ask about the model-dependence of this prediction. The transverse amplitude has model sensitivity in its Q^2 dependence and depends on model ingredients, however, there are no quark model predictions that would come even close to the predictions of the hybrid quark-gluon model. The radial excitation of the Roper resonance gives a qualitatively different prediction for $A_{1/2}(Q^2)$ compared to the hybrid excitation, where the 3-quark component remains in the ground state with only a spin-flip occurring (just as for the $N-\Delta(1232)$ transition. The suppression of the longitudinal coupling, i.e. $S_{1/2}(Q^2) = 0$, is a property of the γqG vertex and is largely independent of specific model assumptions.

These studies have so far only be done for the two states $N(1440)\frac{1}{2}^+$ and $\Delta(1600)\frac{3}{2}^+$. The latter state was considered as a candidate for the lowest mass gluonic Δ_G. A result similar to the one for the hybrid Roper is found in [14] for a hybrid $\Delta_G(1600)\frac{3}{2}^+$, i.e. a fast falling $A_{1/2}(Q^2)$ and $S_{1/2}(Q^2) \approx .0$. The amplitudes at the photon point are not inconsistent with the quark model calculation but are inconsistent with the hybrid baryon hypothesis. This result is also in line with the expectation that the lowest mass hybrid states should have considerably higher masses than the first radially excited quark states. Note that there are currently no data for the Q^2 dependence of the $A_{1/2}$ and $S_{1/2}$ amplitudes of this state.

III. EXPERIMENTAL ASPECTS

A. The CLAS12 detector

The experimental program will use the CLAS12 detector shown in Fig. 3 for the detection of the hadronic final state. CLAS12 consists of a Forward Detector (FD) consisting of six symmetrically arranged sectors defined by the six coils of the toroidal superconducting magnet. Charged particle tracking is provided by a set of 18 drift chambers with

a total of 36 layers in each sector. Additional tracking at $5^\circ - 35^\circ$ is due to a set of 6 layers of micromesh gas detectors (micromegas) immediately down stream of the target area and in front of the High-Threshold Cherenkov counter (HTCC). Particle identification is provided by time-of-flight information from two layers of time-of-flight detectors. Electron, photon and neutron detection are provided by the triple electromagnetic calorimeter, PCAL, EC(inner) and EC(outer). The heavy gas Cherenkov counter (LTCC) provides separation of high momentum pions from kaons and protons. The Central Detector (CD) consists of 6-8 layers of silicon strip detectors with stereo readout, 6 layers of micromegas, arranged as a barrel around the target, 48 scintillator bars to measure particle time-of-flight detector from the target (CTOF), and a central neutron detector. Further details on all CLAS12 components (magnets, detectors, data acquisition, software) may be obtained from: https://www.jlab.org/Hall-B/clas12-web/.

A polarized electron beam will be scattered off a liquid hydrogen target. The scattered electrons will be detected in the forward detectors of CLAS12 for scattering angle greater than about 6°. Momentum reconstruction will be done in the drift chamber system consisting of 36 layers of drift chambers, which are localized in 3 regions called R1, R2, and R3. Additionally, tracking will make use of the 6 layers of the forward micromegas tracker (FMT), which will improve vertex reconstruction and overall angle and momentum resolution. Electron identification uses the high threshold Cerenkov Counter (HTCC), the pre-shower calorimeter (PCAL), and the electromagnetic calorimeter (EC). Timing hits in the forward time-of-flight system (FTOF) will also be required. Electrons scattered at angles from $2.5^\circ - 4.5^\circ$ will be detected in the lead-tungstate calorimeter and the scintillation hodoscope and tracked in a double layer of micromegas tracker. The use of both the FT and CLAS12 to detect scattered electrons provides coverage in a wide range in Q^2, from quasi-real photons at $Q^2 = 0.05 - 0.6\text{GeV}^2$ and at $Q^2 = 0.7$ to 10GeV^2. Charged hadrons will be measured in the full range from $6^\circ - 130^\circ$ with the polar angle acceptance depending somewhat on their charges. Detection of high-energy photons is possible for polar angles from $2.5^\circ - 35^\circ$ using the PCAL and EC as well as the FT calorimeter. At an operating luminosity of $L = 10^{35}\text{cm}^{-2}\text{s}^{-1}$ hadronic rates of $5\text{x}10^6\text{s}^{-1}$ are expected.

B. The Forward Tagger

An essential component of the hadron spectroscopy program with CLAS12 is the Forward Tagger (FT) shown in Fig 4. The FT uses a high resolution crystal calorimeter composed of 324 lead-tungstate crystals to measure the scattered electrons in the polar angle range of 2.5° to 4.5°, and with full coverage in azimuthal angle. The calorimeter measures electron and photon energies with an energy resolution of $\sigma(E)/E \leq 0.02/\sqrt{E} \oplus\ 0.01$. The fine granularity of the calorimeter also provides good polar angle resolution. A 2-layer tiles scintillator hodoscope is located In front of the calorimeter for the discrimination of photons. A four-layer micromegas tracker will be used for precise electron tracking information.To discriminate charged and neutral particles two layers of a scintillator tiles hodoscope and four layers of a micromegas tracker are incorporated in front of the calorimeter. Electron detection in the FT will allow probing the crucial Q^2 range where hybrid baryons maybe identified due to their fast drop in the $A_{1/2}(Q^2)$ amplitude and the suppression of the scalar $S_{1/2}(Q^2)$ amplitude.

Construction of the FT is currently underway at INFN/Genova (Italy), CEA/Saclay (France), and the University of Edinburgh(UK). The FT is expected to be ready for shipment to Jefferson Lab and installation in CLAS12 in the fall of 2015.

IV. SIMULATIONS

In order to have a realistic account of the acceptance for the processes we want to study, two event generators were developed for the processes $ep \to e'K^+\Lambda$ (and $\Lambda \to p\pi^-$) and $ep \to e'p\pi^+\pi^-$, respectively. Both reactions have four charged tracks and the event pattern coming from resonance decays maybe quite similar. To the degree possible the event generators have been tuned on existing data, mostly from CLAS. However, extrapolations to high W and very small Q^2 have been necessaryy, where no prior data exist. The generator for $ep \to e'p\pi^+\pi^-$ has been initially used to determine the most efficient configuration for beam energy and Torus magnet setting in terms of field polarity and current.

A. Event generator for $ep \to ep\pi^+\pi^-$

The Monte Carlo simulation of $\pi^+\pi^-p$ exclusive electroproduction was carried out in the area of invariant masses of the final hadron system W from 2π production threshold to 3 GeV and at photon virtualities Q^2 from 0.05 GeV^2 to 2.0 GeV^2. The GENEV event generator that employs five-fold differential cross sections from the JM05-version [21–23] of the meson-baryon model JM was used. The JM05 model version incorporates reaction mechanisms, that

are sufficient for a realistic simulation of the event distributions in the reaction phase space. The generated events are shown in Fig. 5.

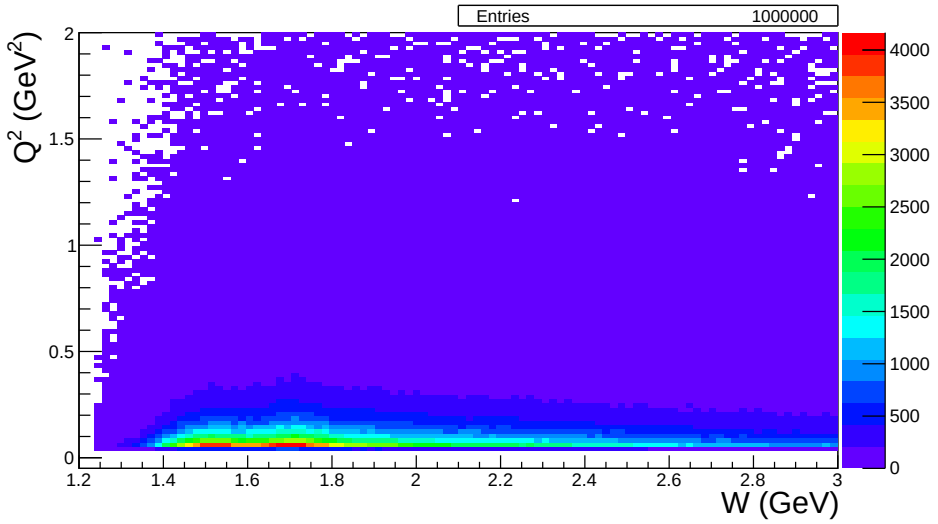

FIG. 5: Q^2 vs W distribution for the generated $\pi^+\pi^-p$ events with the electron beam energy 6.6 GeV. The GENEV event generator based on JM05 [21–23] model was used to generate 10^6 events.

All studies described above were performed with the GENEV version of 2π event generator, which is written on FORTRAN and has several limitations. It employs $\pi^+\pi^-p$ differential cross sections from the old JM05 version of the JM model [21–23]. During the past several years the model was further developed [**?**] and significantly improved. Furthermore, the 2-pion part of the GENEV is applicable only up to 2 GeV over W and from 0.3 GeV^2 over Q^2, and in the region of interest (high W and low Q^2) it uses simple interpolations. The effort with the goal of developing a new event generator for the simulation of the $\pi^+\pi^-p$ electroproduction off protons is currently underway. The new event generator will employ the 5-fold differential cross sections from the recent version of the JM15 model fit to all results on charged double pion photo-/electroproduction cross sections from the CLAS both the published and preliminary [25–28]. It will provide output in the format compatible with the new CLAS12 reconstruction software.

In the W range from 1.4 GeV to 1.8 GeV and Q^2 from 0.65 GeV^2 to 1.3 GeV^2 the new generator succesfully reproduces available integrated and single differential 2π cross sections [25]. The quality of the description is shown in Fig. 6. In order to extend kinematical coverage toward extremely low Q^2 integral cross section of 2π photoproduction were used [28]. The resulting Q^2 dependence of the total cross section is shown in right plot of Fig. 6. The next step of the event generator development will be an extension of the kinematical coverage to the area of higher W up to 2.5 GeV.

We expect more precise results on expected run condition and estimations of event rates using new event generator to be available within 6 months.

B. Acceptance estimates for $ep \to ep\pi^+\pi^-$

For the event reconstruction a simplified version for the CLAS12 event reconstruction software, the so-called FASTMC routine was employed to filter the generated events for acceptance. This routine accounts for the detector fiducial areas and provides smearing over the final particle angles and momenta. The accepted events are shown in Fig. 7 plotted Q^2 vs W. The different panels show distributions for reconstructed $\pi^+\pi^-p$ events at various beam energies. The torus current was set to +3375 A, which leads negatively charged particles to bend towards the beam line. The area of zero acceptance seen in the plots represent the gap between the Forward Tagger and the minimum polar angle accepted in CLAS12 for intending particles. For the hybrid baryon search the area of small photon virtuality is of particular interest. The size of the gap depends on the Torus current setting and the momentum of the scattered electrons. For a negative Torus current, i.e. outbending electrons the gap is simply given by the geometrical acceptance of CLAS12 and is largely independent of the particle momentum, while for inbending particles the acceptance depends on scattering angle, particle momentum, and magnetic field strength. The acceptance for electron scattering angles from 2.5 to 4.5 degrees, which is covered by the FT, is independent of the Torus magnet settings. In order to cover photon virtualities as low as to 0.05 GeV^2 measurements with 6.6 GeV electron beam

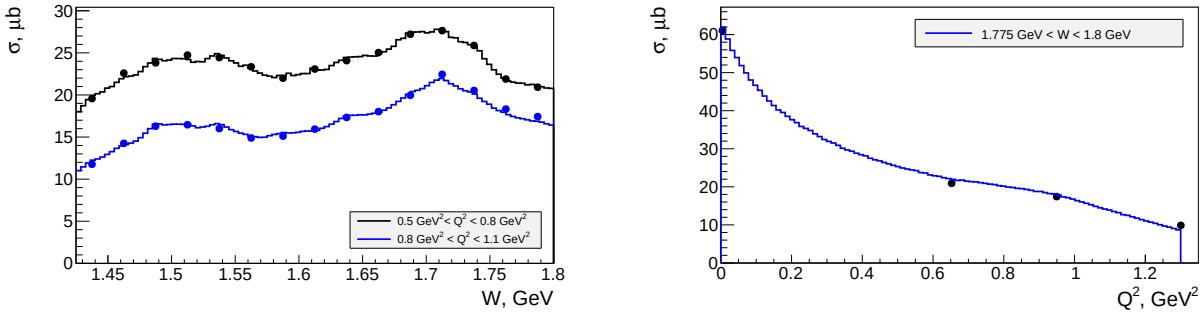

FIG. 6: Comparison between event distributions from new two pion event generator (curves) and integrated cross sections from recent version of JM model [24] (points). Left plot shows W dependence of total cross section for two Q^2 bins in comparison with the model in two Q^2 points 0.65 GeV^2 and 0.95 GeV^2. Right plot shows Q^2 dependence of total coss section for one W bin in comparison with JM model at $W = 1.7875$ GeV. The first point at $Q^2 = 0$ GeV^2 corresponds to the unpublished photoproduction data [28]. While three other points correspond to the data [25].

energy is required. The minimal Q^2 values for reconstructed events increase up to 0.13 GeV^2 and 0.2 GeV^2 for beam energies 8.8 GeV and 11 GeV, respectively.

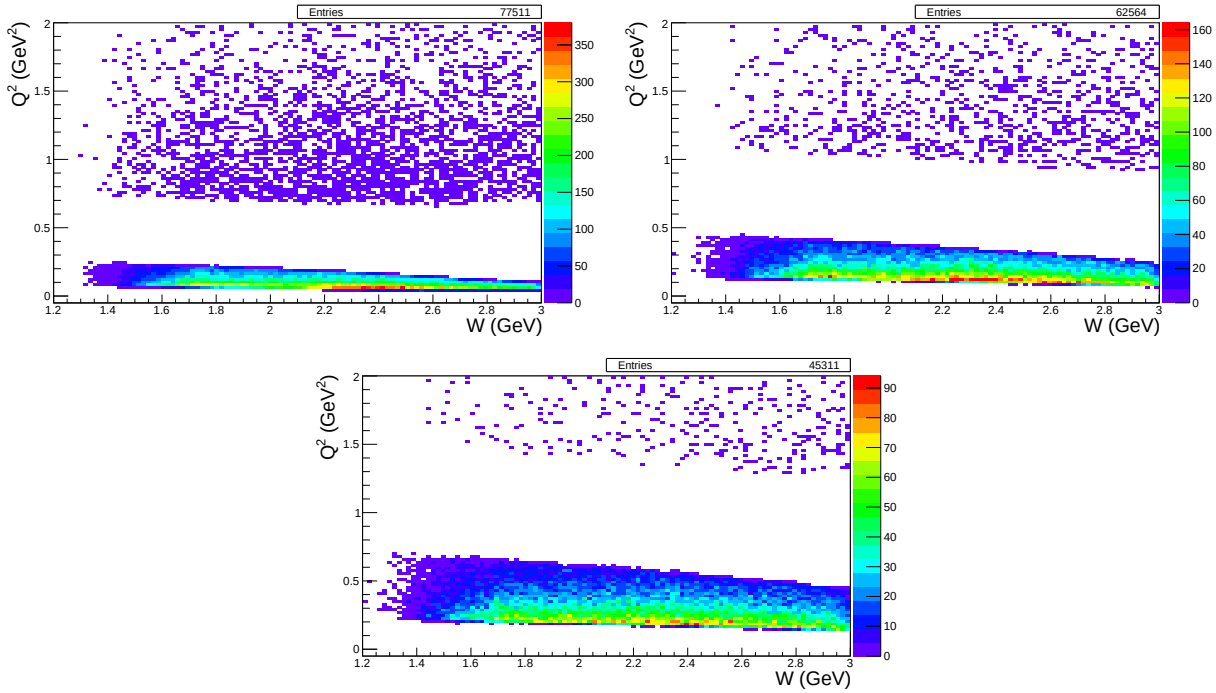

FIG. 7: Q^2 vs W distributions for the reconstructed $\pi^+\pi^-p$ events (all particles in final state are registered). Top left, right, and bottom plots correspond to 6.6 GeV, 8.8 GeV, and 11 GeV beam energies, respectively.

With the beam energy 6.6 GeV, the influence of the magnetic field direction on the accessible kinematical coverage for the $\pi^+\pi^-p$ electroproduction was further studied. The Q^2 vs W distributions for reconstructed $\pi^+\pi^-p$ events are shown in Fig. 8 for the two opposite polarities of the torus current, +3375 A and -3375 A. A wide area of zero acceptance is clearly seen for the normal (+3375 A) direction of the magnetic field in Fig. 8 (left). Reversing magnetic field allows us to decrease substantially the inefficient area, as it is shown in Fig. 8 (right). Therefore, the reversed magnetic field represents the best configuration for the proposed experiment, as well as for other experiments for which the area of small photon virtualities is of particular interest.

We also explored the evolution of counting rate as the function of the magnetic field strength. The 2D Q^2 vs W distributions for the accepted $\pi^+\pi^-p$ events are shown in Fig. 9 for the torus currents: -3375 A (left) and -1500 A (right), that correspond to the full and half strengths of the magnetic field for the CLAS detector. For the CLAS12

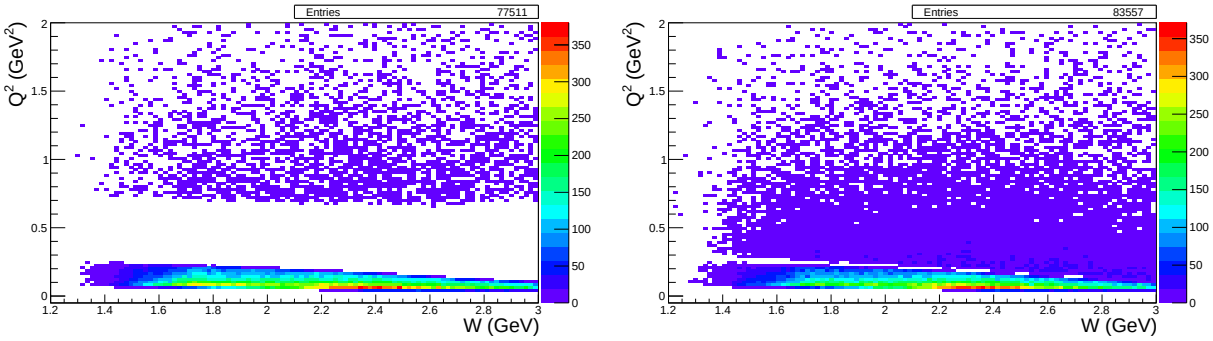

FIG. 8: Q^2 vs W distributions for reconstructed $\pi^+\pi^-p$ events (all particles in final state are registered) for the torus currents +3375 A (left) and -3375 A (right). The reversed magnetic field closes the gap between Forward Tagger and CLAS12.

the maximum value of torus current is expected to be 3770 A. According to the results in Fig. 9, counting rate should increase by almost a factor of two at half strength of the magnetic field, because of the improved acceptance for the detection of the three $\pi^+\pi^-p$ particles in the final state and the scattered electron. While the particle momentum resolution will be negatively affected at lower field, a 50% to 60% value of the CLAS12 torus field might be a good compromise between good momentum resolution and large acceptance or the proposed measurement.

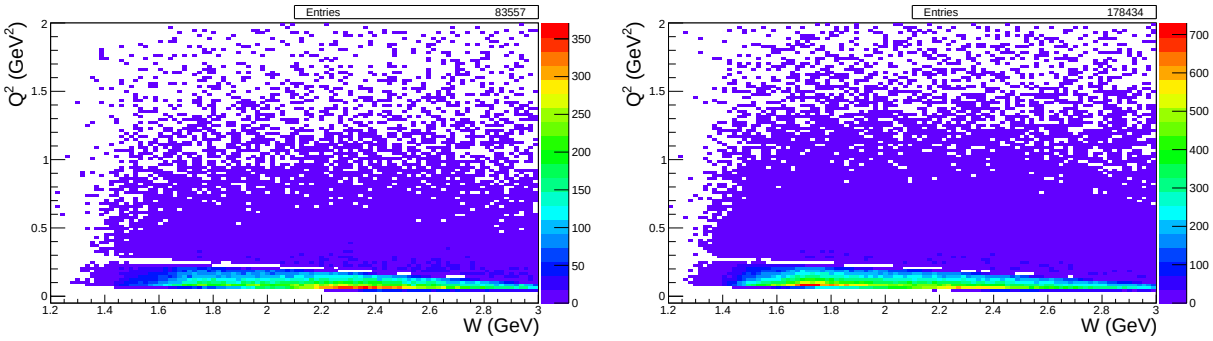

FIG. 9: Q^2 vs W distributions for reconstructed $\pi^+\pi^-p$ events (all particles in final state are registered) with the torus currents: -3375A (left) and -1500A (right). With lower torus current significantly more events are reconstructed.

C. Resolution in hadronic mass reconstruction and background estimation

The resolution in the hadronic mass is of particular importance in the studies of excited nucleon states, since this quantity determines the capability for reliable isolation of the resonant contributions in exclusive cross sections. For a credible separation between the resonant and the non-resonant contributions the resolution over W should be much smaller than the N* decay width. Typical values for the decay widths of nucleon resonances with masses $>$ 2.0 GeV are in a range from 250 to 400 MeV. A mass resolution of $\approx$ 25 MeV is sufficient for the reliable isolation of contributions from hybrid-baryons that are expected in the mass range from 2.0 to 3.0 GeV. The resolution in W for the reconstructed $\pi^+\pi^-p$ events was studied in the following way. For each reconstructed event we compute the difference between the exact W_{gen} and the reconstructed W_{rec} W-values. We compare the two ways of determining the invariant mass of the final hadron system: a) from the difference between the four-momenta of the initial and the scattered electrons that was added to the four-momentum of the target proton (electron scattering kinematics); b) from the sum of the four-momenta of the final π^+, π^-, and proton (hadron kinematics). The reconstructed $\pi^+\pi^-p$ event distributions over the difference $W_{gen} - W_{rec}$ provide information on the resolution over W. The aforementioned distributions for the electron scattering and hadron kinematics are shown in Fig. 10. Beam energy was set to 6.6 GeV, torus current was set to -1500 A. For both ways of determining W_{rec} value, the resolution over W is better than 25 MeV and sufficient for the separation of resonant/non-resonant contributions. If W_{rec} ($= \sqrt{s}$) is computed from the hadron kinematics, the resolution is significantly better than in a case of electron scattering kinematics. However, the hadron kinematics requires the registration of all final hadrons with registration efficiency much lower than in a case, when the value of W_{rec} is determined from the electron scattering kinematics.

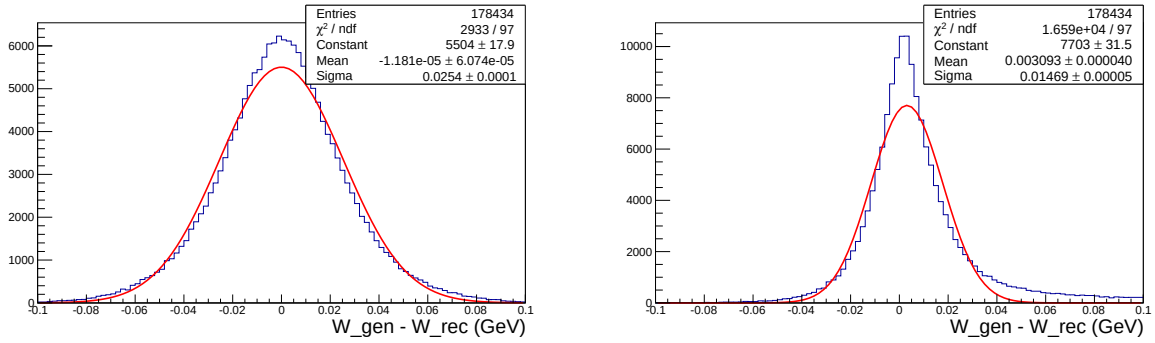

FIG. 10: The distributions of the reconstructed $\pi^+\pi^-p$ events over the value $W_{gen} - W_{rec}$ for W_{rec} determined in electron scattering (left) and hadron (right) kinematics. See text for explanation of both kinematics.

The studies of charged double pion electroproduction with the CLAS detector [25, 27] demonstrated that the topology, when the final π^- is not detected and its four-momentum is reconstructed from the energy-momentum conservation provides the dominant part of the statistic. We expect that topologies when one of the final pion is not detected will provide the dominant statistic also in the proposed experiment. We are planning to select the $\pi^+\pi^-p$ events employing the exclusivity cuts over missing mass squared distributions for the final π^+ and π^-. The contribution from other exclusive channels (exclusive background) to the events within the exclusivity cuts was evaluated in the Monte-Carlo simulation. Most of the exclusive background events come from the $ep \to e'p'\pi^+\pi^-\pi^0$ channel. Both $\pi^+\pi^-p$ and 3π events were generated with the relative contribution from 3π events of $\approx 9\%$. The phase space distribution was assumed for the 3π events. With this mixture of generated events we reconstructed the $\pi^+\pi^-p$ events and determine their distribution over missing mass squared for π^+ and π^-. They are plotted in Fig. 11. Blue curves on Fig. 11 show 2π events contribution, green curves stand for the 3π events contribution. The exclusivity cuts provide excellent isolation of the $\pi^+\pi^-p$ events with almost negligible contribution from the 3π events.

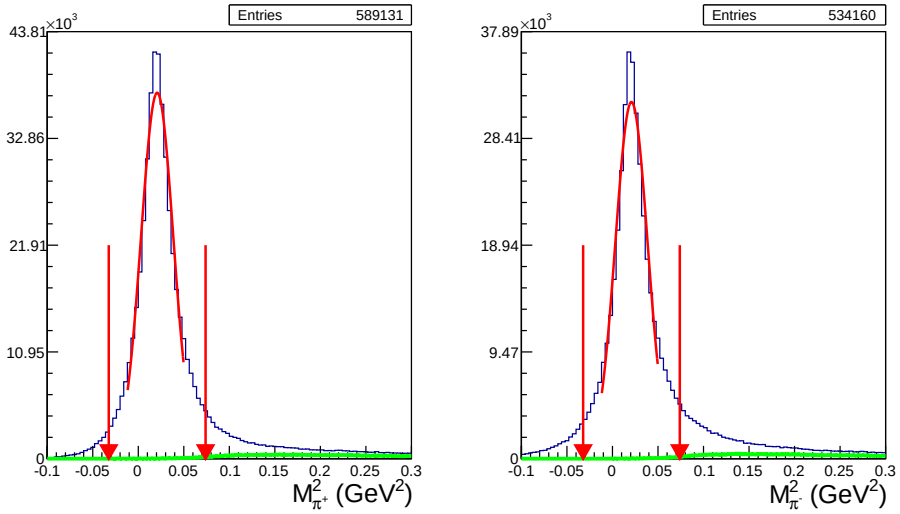

FIG. 11: The reconstructed $\pi^+\pi^-p$ event distributions over the missing masses squared of π^+ (left) and π^- (right) for the generated $\pi^+\pi^-p$ events with admixture of 9% from 3π events. The contributions from the $\pi^+\pi^-p$ and the $\pi^+\pi^-\pi^0p$ events are shown by blue and green curves, respectively. Red arrows show the exclusivity cuts applied.

D. Summary of experimental condition study

Summary of the run conditions studied in the simulations described above is listed in Table I. The bottom row corresponds to the optimal set-up for the proposed experiment.

Summary of the kinematical coverage in terms of 2D φ vs θ distributions for the final hadrons are shown on Fig. 12 with all final hadrons detected, beam energy equal to 6.6 GeV and torus current -1500 A. Vertical strip around

Energy (GeV)	Current (A)	Eff. all reg.	Eff. π^+ miss (%)	Eff. π^- miss(%)	miss. π^+	miss. π^-	Q^2_{min}	σ(W)	$\sigma(\sqrt{s})$
11	+3375	4.5					0.2	34	16
11	-3375	4.2					0.2	34	15
11	+1500	8.4					0.2	36	16
11	-1500	8.3					0.2	36	16
8.8	+3375	6.2					0.13	29	16
8.8	-3375	6.1					0.13	29	15
8.8	+1500	12.2					0.13	31	15
8.8	-1500	12.5					0.13	31	16
6.6	+3375	7.8	13.4	12.3	0.21	0.28	0.05	23	15
6.6	-3375	8.4	17.0	12.9	0.21	0.26	0.05	25	14
6.6	+1500	16.0	21.2	21.0	0.14	0.18	0.05	23	15
6.6	**-1500**	**17.8**	**25.0**	**21.4**	**0.23**	**0.23**	**0.05**	**25**	**15**

TABLE I: Comparison of run conditions for the $\pi^+\pi^-p$ channel. The highlighted bottom row represents the optimal run condition for the 6.6 GeV beam energy..

$\theta = 40$ deg in all plots in Fig. 12 corresponds to the gap between Forward and Central parts of CLAS12 detector. Since reversed torus magnetic field was chosen, low θ angle area is more populated for negatively charged particles (π^-).

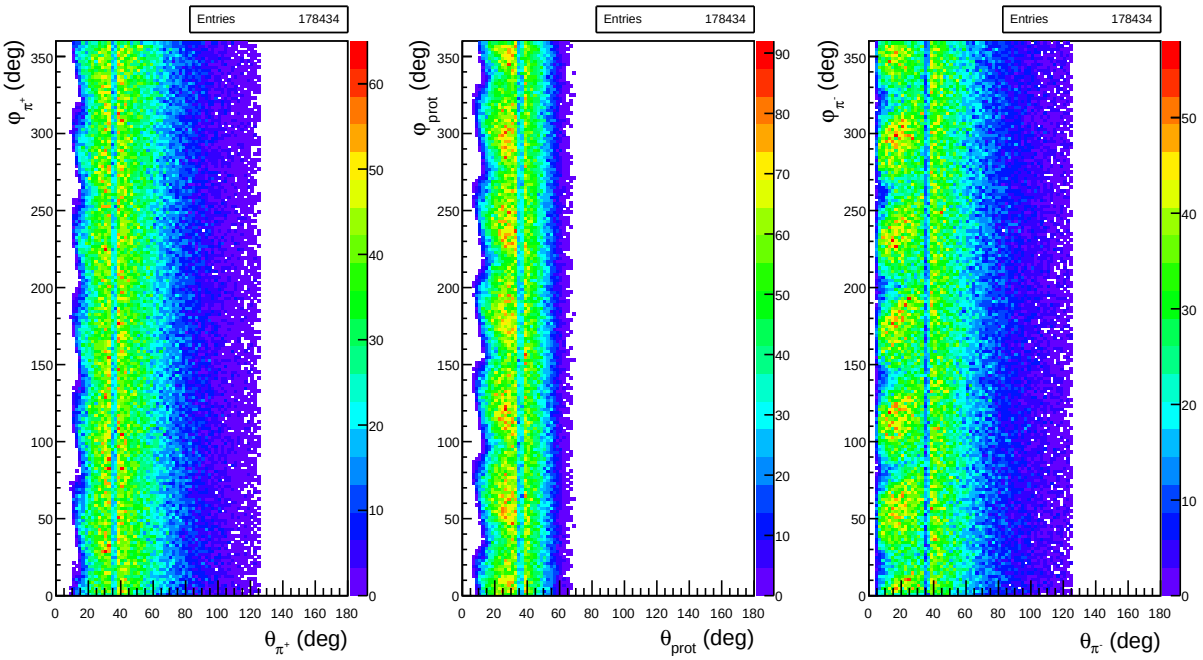

FIG. 12: φ vs θ distributions for the final hadrons: π^+ (left), proton (middle), and π^- (right).

E. The $K\Lambda$ and $K\Sigma$ event generators

The $ep \to e'K^+\Lambda$ event generators is based on model cross section calculations. The models [16] for $K^+\Lambda$ and [17] for $K^+\Sigma^0$ channels describe KY electroproduction in the framework of a Regge-plus-resonance approach. Resonance contribution in s-channel is described with the help of effective-Lagrangian approach and the background part of the amplitude is modeled in terms of t-channel Regge-trajectory exchange.

Comparison of the fully integrated model cross section with experimental CLAS data is demonstrated in Figs.13. The cross sections are presented as a function of Q^2 for a given bin in $W = 2.05$ GeV. Differential cross sections in certain bins of Q^2 , W are shown in Figs. 14 and Figs. 15. The model reasonably reproduces experimental data for $0.65 < Q^2 < 1.5$ GeV^2, while it considerably underestimates the cross section for $Q^2 > 1.5$ GeV^2. It does not create

problems since our region of interest if low Q^2 values. We rely on the model cross section for $Q^2 < 0.65$ GeV^2, as there are no experimental data to compare to. Calculated cross section is more sensitive to the distributions of event generator in the regions with sharp bumps. We can see in Figs. 14, 15 that the model reproduces well the general features of the cross section growth at large cos(θ) for Q^2 >1.5 GeV^2. and W >2.0 GeV^2.

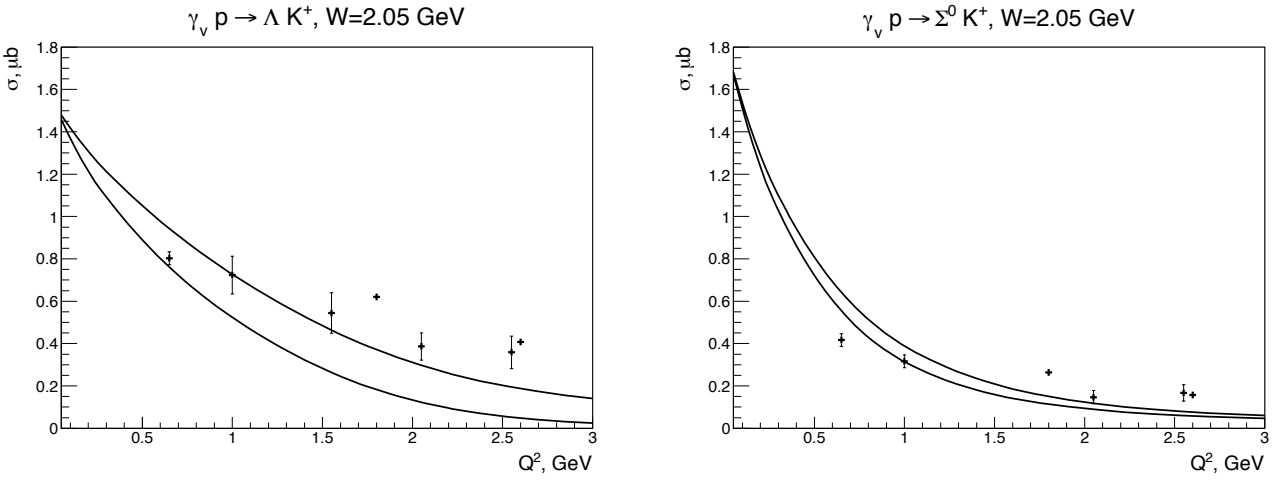

FIG. 13: Integrated cross section for $K^+\Lambda$ (left) and $K^+\Sigma^0$ (right) channel as a function of Q^2 at $W = 2.05$ GeV. Experimental cross sections at Q^2 =0.65 GeV are measured with energy 2.567 GeV. Cross sections at $Q^2 = 1.8$ and 2.6 GeV are measured with beam energy 5.5 GeV. Other points correspond to the beam energy 4.056 GeV. For $K^+\Sigma$ model calculations are shown in two curves: upper curve is for beam energy 2.567 GeV and lower curve is for 5.5 GeV.

F. Acceptances for $ep \to e'pK^+\Lambda$

In Figs. 16 and in Figs. 17 we compare the angular distributions for the +1500 A and the -1500 A Torus currents. in Figs. 16 we see qualitatively the same behavior as for the $p\pi^+\pi^-$ final state: inbending electrons generated in an W interval from $K^+\Lambda$ threshold at 1.6 GeV to 3.5 GeV and scattering angles $\theta_e \geq 2^\circ$ are detected in CLAS12 starting at about 6.5° with the acceptance opening up towards larger scattering angles. The stripe-like pattern in seen in the accepted protons and K^+ is due to the azimuthal motion of charged tracks in the strong solenoid field that generates a "kick" in azimuth that depends on the production angle and the particle momentum. It should be noted that the particles are not traversing the sectors in this pattern, as the plotted quantities are the values at the production vertex. The pattern for the π^- is different as they have on average much lower momentum and their migration in ϕ is larger and more diffuse. For production on hydrogen, the recoil protons are kinematically limited to polar angles of about $\leq 65^\circ$. Figs. 17 show the acceptances for out-bending electrons for which the acceptance in CLAS12 is rather uniform in azimuth and full acceptance sets in for scattering angles at 5.5°. As a result the event acceptance for this configuration is more than a factor 2 larger than for the in-bending field configuration. We also note that for both configuration there exists a band in polar angle from 35° to 40° where the acceptance is depleted. This is due to a partially blind transition region between the forward detectors and the central detectors.

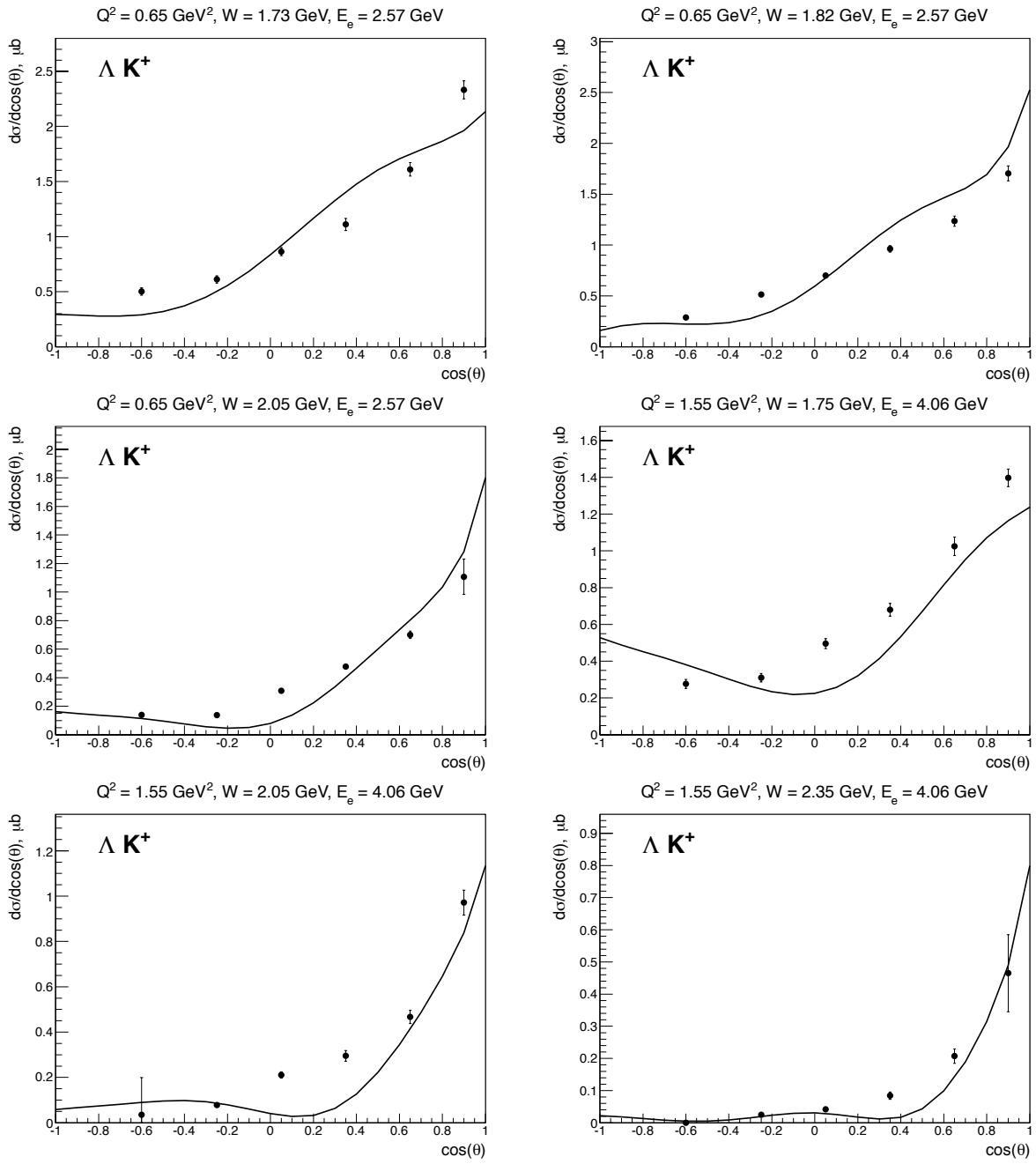

FIG. 14: Differential cross sections for for $K^+\Lambda$ channel in certain bins of Q^2, W for some beam energies. θ is polar angle of a kaon in CMS.

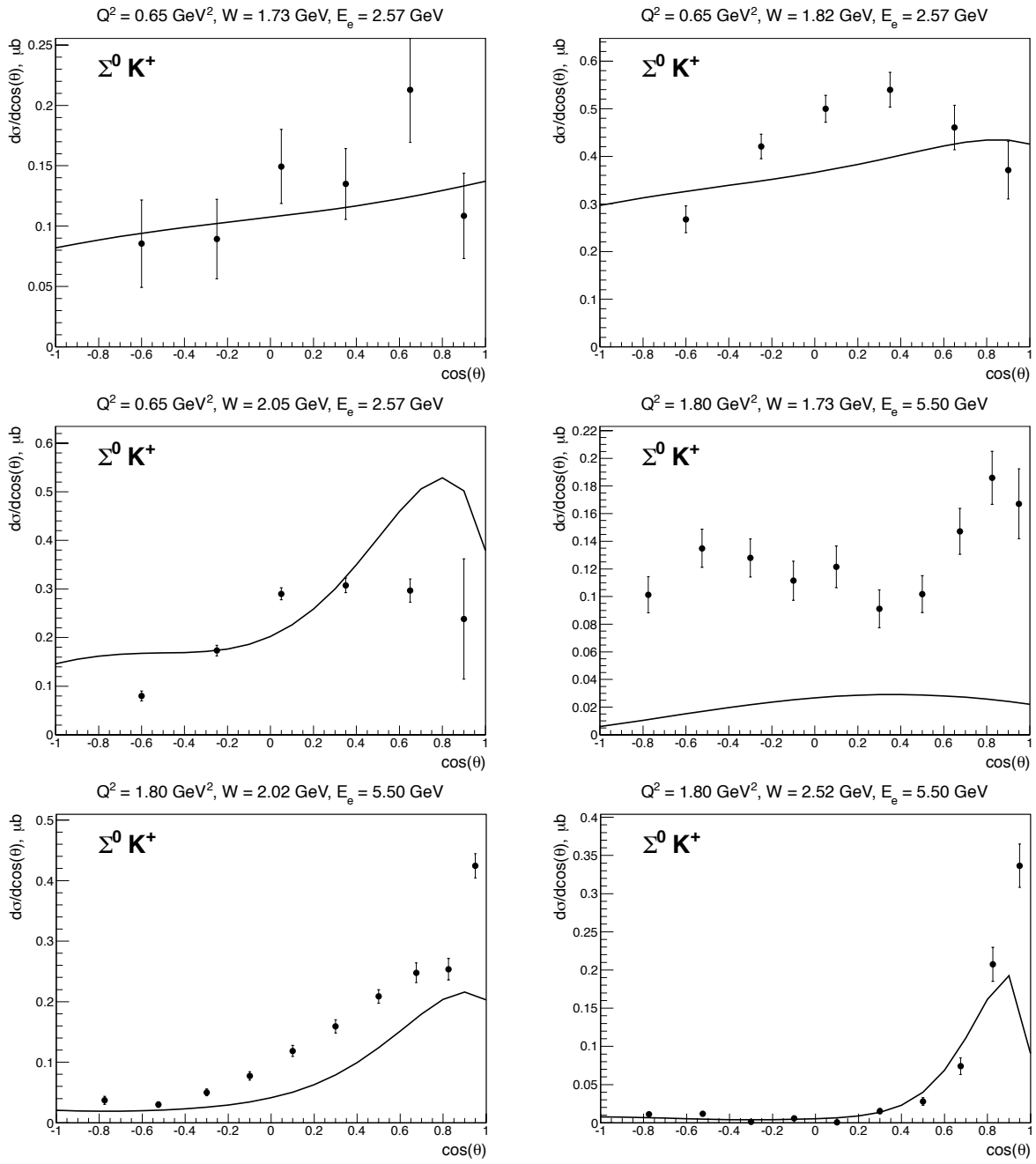

FIG. 15: Differential cross sections for for $K^+\Lambda$ channel in certain bins of Q^2, W for some beam energies. θ is polar angle of the kaon in CMS.

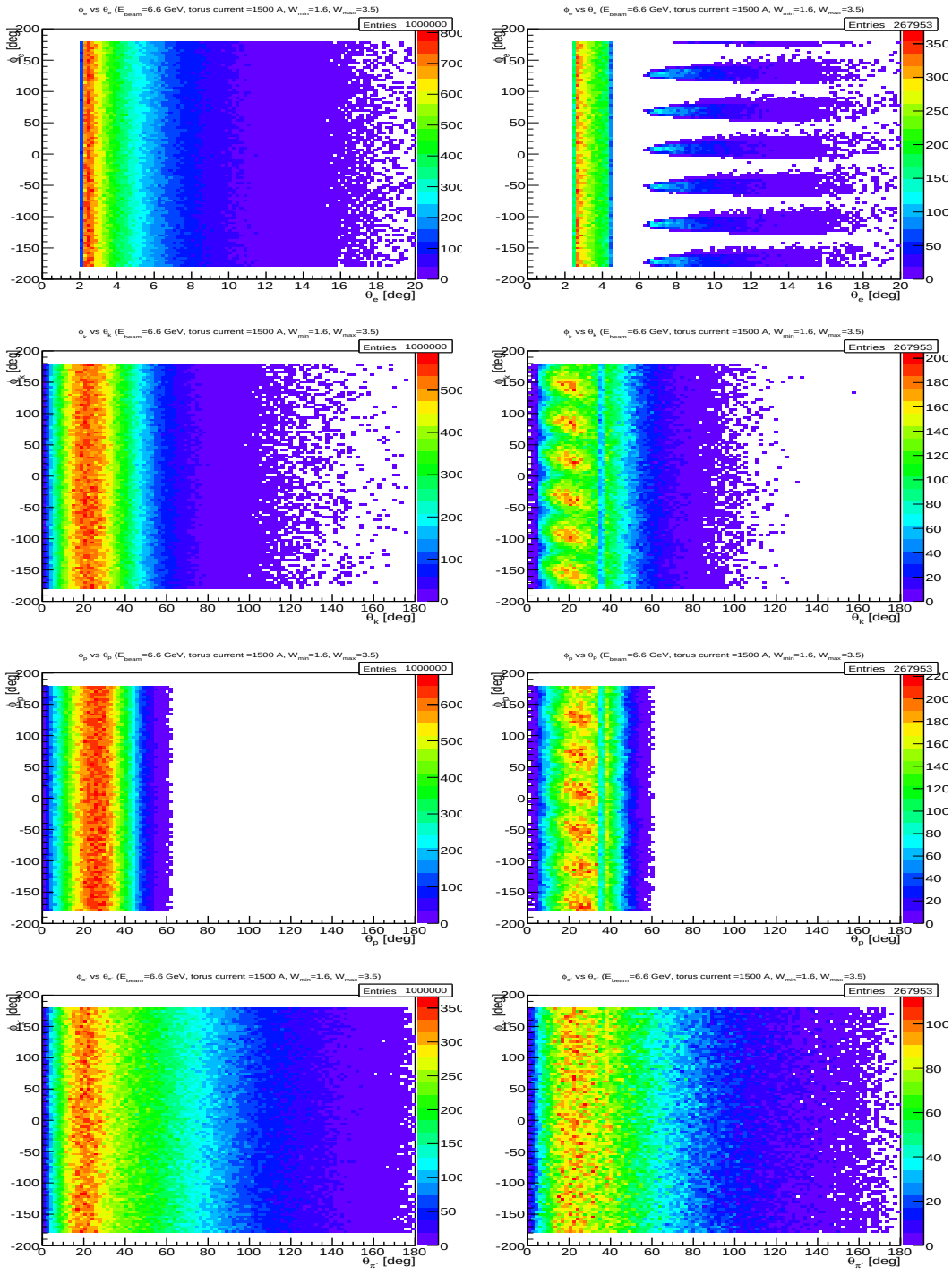

FIG. 16: Azimuthal versus polar angle of generated (left) and accepted events (right) for electrons (top row), K^+ (2nd row), protons (third row), and π^- (bottom row). Events are generated in the range W from 1.6 to 3.5 GeV. The Torus current is set I=+1500A, that bends negatively charged particles inwards towards the beamline and reduces the acceptance for electrons within CLAS12

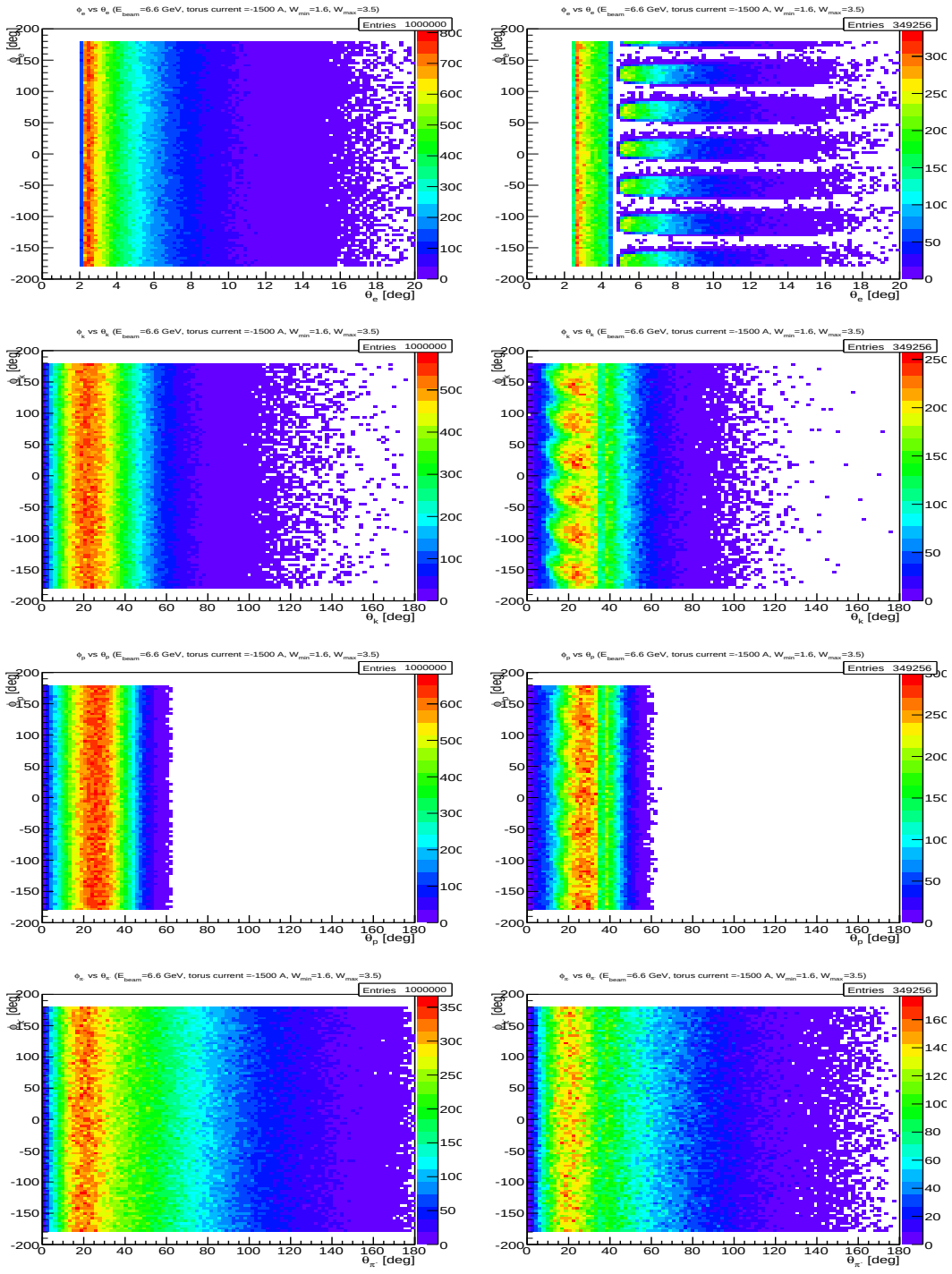

FIG. 17: Azimuthal versus polar angle of generated (left) and accepted events (right) for electrons (top row), K^+ (2nd row), protons (third row), and π^- (bottom row). Events are generated in the range W from 1.6 to 3.5 GeV. The Torus current is set at I=-1500A, that causes negatively charged particles to bend outwards.

G. Count rates from $K^+\Lambda$

The expected total number of KY electroproduction events in the reaction $e_i p_i \to epKY$ can be written as:

$$N = L \cdot t \cdot \int \frac{d^5\sigma}{dE_e d\Omega_e d\Omega_Y^*} dE_e d\Omega_e d\Omega_Y^* \,, \tag{1}$$

where

- $L = 1 \times 10^{35}\,\mathrm{cm}^{-2}\mathrm{c}^{-1}$ is expected CLAS12 operating luminosity
- t is expected run time.
- $\frac{d^5\sigma}{dE_e d\Omega_e d\Omega_Y^*}$ is the cross section from (**??**).

Integration in (1) is performed over the whole kinematics space. The event rate R is defined as $\frac{N}{t}$.

Integration in (1) can be done numerically using model cross section for $d^2\sigma/d\Omega_Y^*$. The minimum achievable value of Q^2 in CLAS12 is determined by the forward hole, where high energy electrons can not be detected. For any beam energies Q^2 is greater than 0.01 GeV. So, we can integrate in (1) given that $Q^2 > 0.01$ GeV. Results of calculation of event rates R_Λ and R_Σ are presented in Table II.

TABLE II: Estimated event rates not taking into account acceptance of CLAS12 for events with $Q^2 > 0.01$ GeV.

E_{beam}, GeV	R_Λ, Hz	R_Σ, Hz
6.6	1500	1200
8.8	1400	1100
11.	1300	900

To account for the acceptance of CLAS12 simulation is needed. We should generate events in the whole kinematics space, but with $Q^2 > 0.01$ GeV then the ratio of reconstructed and generated events gives the averaged acceptance. Multiplying event rates from Table II by that ratio we get event rates which account for the acceptance. An event for the final state $eK^+p\pi^-$ considered to be reconstructed if electron and at least two hadrons have been detected. It is preferable to have two charged hadrons in the trigger as it allows increase statistics for our channels of interest. Event rate calculations are presented in Table III for all possible beam energies and torus currents.

Currently fact MC is used to estimate acceptance. Real simulation and reconstruction will be used in the future.

TABLE III: Estimated event rates taking into account acceptance of CLAS12 for the sub-channel $ep \to eK^+\Lambda \to eK^+p\pi^-$. Electron and two hadrons are required to be accepted.

E_{beam}, GeV; Torr. cur, A	R_Λ, Hz
6.6; +1500	225
6.6; −1500	240
6.6; +2950	135
6.6; −2950	112
8.8; +1500	168
8.8; −1500	168
8.8; +2950	105
8.8; −2950	82
11.; +1500	108
11.; −1500	124
11.; +2950	100
11.; −2950	62

Event rates from Table III may not be feasible in experiment, since the KY production contribute a little to the inclusive cross section. The very rough estimates suggests that KY channel contribution is about 1% with respect to

the two and three pion production. The latter channels are in turn dominant among channels that have an electron and at least two charged hadrons in the final state. Thus, the total even rate is expected to be about $240 \times 100 \approx 20$kHz for the trigger configured so that electron and two charged hadrons are detected. These estimations of event rates are quite approximate, since the model cross section used for KY production as well as ratio of the KY cross section to the two and three pion production cross sections are not known well.

H. Expected event rates

At the very forward electron scattering angles, electron rates will be very high and may exceed the capabilities of the data acquisition system. Therefore additional constraints are needed to reduce the trigger rate. This requires the selection of a hadronic event pattern that should significantly enrich the sample with final state topologies as one might expect from hybrid baryon candidates. For realistic rate estimates, projections of hadronic coupling strengths of hybrid baryons are needed, which are currently not available. For an initial program we therefore consider to trigger on hadronic final states with at least two charged particle. This will cover final states: $K^+\Lambda \to K^+p\pi^-$, $p\pi^+\pi^-$, $p\phi \to pK^+K^-$, $p\eta' \to p\pi^+\pi^-\eta$. In addition, a single charged hadron trigger will be incorporated with a pre-scaling factor that will in parallel collect events with a single charged hadron in the final state, i.e. π^+n, $p\pi^\circ$, $K^+\Lambda$, and $K^+\Lambda$, among others.

The operating luminosity of CLAS12 is estimated at $L = 10^{35} cm^2 sec^{-1}$. This corresponds to an event rate of 700 Hz (for $K^+\Lambda$) and about 500 Hz (for $K^+\Sigma^\circ$). For a 60 days run at that luminosity, the total number of $K^+\Lambda$ events is estimated at 3.2×10^9, and the number of $K^+\Sigma$ events at 2.6×10^9. The number of events in any histogram for certain smaller intervals of Q^2 and W, can be found in the same way. The lowest event rate is expected for high Q^2 and high W. For the kinematics with lowest statistics, e.g. $2.0 \le Q^2 \le 2.5\text{GeV}^2$ and $2.675 \le W \le 2.700$GeV, a total number of 4.0×10^5 $K^+\Lambda$ events, and 2.1×10^5 $K^+\Sigma^\circ$ events is expected.

While these rates seem very large, it should be kept in mind that the signals of hybrid baryons that we want to detect and quantify may be 10 times smaller than the signal from ordinary quark states and will likely not simply be seen as a peak in the excitation spectrum, but rather as a broad region in W where specific quantum numbers, i.e. $I = \frac{1}{2}$, $J^P = \frac{1}{2}^+$ or $J^P = \frac{3}{2}^+$ must be identified, and the electromagnetic couplings must be measured vs Q^2. This can be achieved in a partial-wave analysis that includes other channels into a multichannel fit, such as the Bonn-Gatchina or Jülich/GWU approaches. Other techniques may also be employed. Very high statistics is thus essential, and the transverse and longitudinal photon polarization that is inherent in electron scattering will provide the amplitude interference to enhance the resonant signal.

V. DATA ANALYSIS

A. Event selection

Electrons will be detected both in the Forward Tagger and in the CLAS12 proper. In CLAS12 electrons can be identified at scattering angles above about 5 degrees in the high-threshold Cherenkov counter (HTCC) and in the PCAL and EC calorimeters. Due to the higher Q^2 for electrons detected at larger scattering angles in CLAS12 compared to the FT region, the electron rate is comparatively much lower than the hadronic rate and good electron identification is important.

For electrons detected in the FT the low Q^2 leads to a very high electron rate that completely dominates the event rate in the FT calorimeter and hodoscope. A direct electron identification at the trigger level is not needed. However the complete event pattern may be checked for consistency with that hypothesis in the event reconstruction. Note that the full electron kinematics is measured in the FT calorimeter and the micromegas tracker and charged particle id is provided by the two layer hodoscope in front of the calorimeter.

Charged hadrons ($\pi^\pm$, $K^\pm$ and protons) will be tracked in the drift chamber and micromegas and the silicon tracker and barrel micromegas at large angles, and identified in the CLAS12 time-of-flight detector system. Photons and neutrons are detected at forward angles in the electromagnetic calorimeters (PCAL, EC, FT) and neutrons at large angles in the central neutron detector (CDN).

B. Event reconstruction and event-based analysis.

The raw data will be subjected to the CLAS12 event reconstruction software package CLARA. We intend to extract differential cross section for all processes with 2-body final states, e.g. KY, $N\pi$, $p\eta$, $p\eta'$ and $p\phi$ using simulations

of large amounts of Monte Carlo events to fully understand the acceptances for these processes at the accuracy level required for the partial wave analysis. As for all electroproduction data, the raw cross sections will be subjected to radiative corrections in order to extract the fully corrected differential cross sections. The radiative correction procedure for exclusive processes is well established, and has been used for correcting single $\pi^+ n$ and $p\pi^\circ$ production as well as $K^+\Lambda$ and $K^+\Sigma$ electroproduction employing the exact procedure developed in Ref. [18]. As has been recently demonstrated [15] radiative corrections are very important for the analysis of exclusive processes in terms of resonance excitations as they affect both the polar and azimuthal angular dependencies, and consequently the partial wave analyses based on these processes.

For 3-body final states, such as $p\pi^+\pi^-$, $p\eta\pi^\circ$ we consider event-based analyses techniques, where acceptances will be assigned to each event, and acceptance weighted events will be subjected to a maximum-likelihood fitting procedure. This procedures preserves the full correlations among the final state particles.

C. Partial wave analysis

Using modern partial wave analyses tools several new excited N^* and Δ^* states have been identified or have been significantly improved in their evidence and star rating in the 2012 edition of the Review of Particle Properties (RPP) of the particle Data Group [1]. The use of high statistics photo production data from CLAS of a number of final states, e.g. $K^+\Lambda$, $K^+\Sigma$, $\imath^+ n$, $p\pi^\circ$, including polarization observables was essential in establishing these new evidence. This success has validated the importance of high statistics data sets in the search for new excited states, and has helped re-vitalized the field of hadron spectroscopy. In the analysis of the data to be taken with the program discussed in this letter-of-intent we will make full use of these advanced tools of amplitude and partial wave analysis. Significant progress has also been made in the analysis of electroproduction data where transition form factors have been extracted from several excited states using the high statistics data from CLAS [4, 5, 15]. We expect that these packages will be well-honed by the time the proposed data will be taken, including the extension of the photoprodcution analysis to include the existing and planned electroproduction data sets.

D. Strategies for identifying Hybrid Baryons

In this section we address the question if and how gluonic hybrid baryons are distinct from ordinary quark excitations. As discussed in section II B the lowest hybrid baryons should have isospin $I = \frac{1}{2}$ and $J^P = \frac{1}{2}^+$ or $J^P = \frac{3}{2}^+$, and their masses should be in the range 2.20-2.50 GeV. This mass range must be verified once LQCD calculations with physical pion masses become available, as this range may shift with more realistic pion masses, likely to the lower mass range. Four states with $I = \frac{1}{2}$ and $J^P = \frac{1}{2}$ are prodicted with dominant quark excitations and with masses below the mass of the lowest hybrid states. Of these four states two are the well known $N(1440)\frac{1}{2}^+$, and $N(1710)\frac{1}{2}^+$, and two are the less well established $N(1880)\frac{1}{2}^+$ and $N(2100)\frac{1}{2}^+$ with 2* and 1* ratings, respectively. Another state $N(2300)$ has a 2* rating, and falls right into the lowest hybrid mass band projected by LQCD. This state, if confirmed, could be the predicted lowest hybrid state.

In order to address this question, it is necessary to confirm (or refute) the existence of the 2* state $N(1880)$ and the 1* state $N(2100)$, as well as, measuring the electromagnetic couplings of $N(2300)$ and its Q^2 dependence. Improved information on the lower mass states should become available in the next one or two years when the new high-statistic single and double polarization data from CLAS have been included into the multi-channel analyses frameworks, such as the Bonn-Gatchina or Jülich/GWU approaches. Should these two states be confirmed, then any new nucleon state with $J^P = \frac{1}{2}^+$ which happens to be in the right mass range, would be a candidate for the lowest mass hybrid baryon. The $N(2300)\frac{1}{2}^+$ state has been seen at BES III only in the invariant mass $M(p\pi^\circ)$ of $\Psi(2S) \to p\bar{p}\pi^\circ$ events. In this case the production of $N(2300)$ occurs at very short distances as it involves heavy quark flavor $c\bar{c}$ creation. Hence the state may even be observable in single pion electroproduction $ep \to e'\pi^+ n$ and $ep \to e'p\pi^\circ$ at high Q^2, if its photocouplings is sufficiently strong to be measurable.

In the $J^P = \frac{3}{2}^+$ sector the situation is more involved. There are two hybrid states predicted in the mass range 2.2 to 2.4 GeV, with masses above five quark model states at same J^P. Of the five states, two are well known 4* and 3* states, $N(1720)\frac{3}{2}^+$ and $N(1900)\frac{3}{2}^+$, and one state, $N(2040)\frac{3}{2}^+$, has a 1* rating. Here we will have to confirm (or refute) the 1* star state and find two or three (if N(2040) is not existing) more quark model state with same quantum numbers in the mass range 1.7 to 2.1GeV. There is one candidate $\frac{3}{2}^+$ state with mass near 1.72 GeV seen in $p\pi^+\pi^-$ electroproduction [25], whose existence we will be able to examine with the expected very high statistics data.

Expected signatures of the lowest mass hybrid baryons:

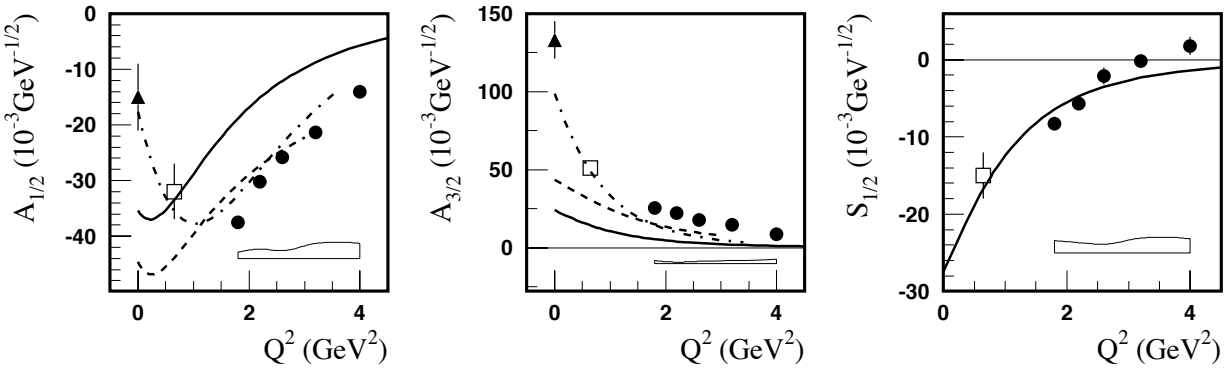

FIG. 18: Electrocoupling amplitudes of the $N(1680)\frac{5}{2}^+$ resonance.

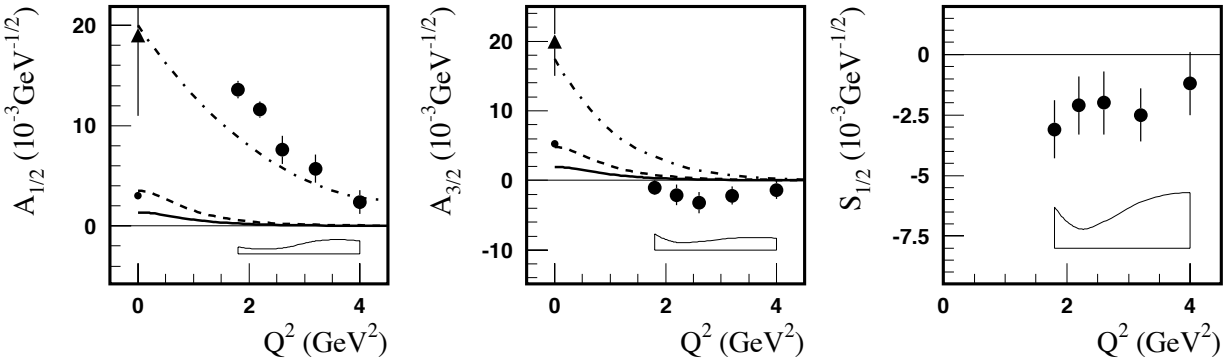

FIG. 19: Electrocoupling amplitudes of the $N(1675)\frac{5}{2}^-$ resonance. Quark models predict the transverse amplitudes to be suppressed. The significant deviation of the $A_{1/2}$ amplitudes is consistent with meson-baryon contributions to the excitation strength (dashed-dotted lines).

- resonances masses in the range $2.2 \leq W \leq 2.5$GeV with $I = \frac{1}{2}$, and $J^P = \frac{1}{2}^+$ or $J^P = \frac{3}{2}^+$
- Q^2 dependence of the transverse helicity amplitude $A_{1/2}(Q^2)$ similar to the $\Delta(1232)\frac{3}{2}^+$ but dissimilar to radially excited states of same J^P.
- Strongly suppressed helicity amplitude $S_{1/2}(Q^2) \approx 0$ in comparison to other ordinary 3-quark states or meson-baryon excitations.

While these signatures maybe used to identify gluonic baryon excitations, the expected high statistics data will be used to identify any new or poorly known state whether or not it is a candidate for a hybrid baryon state. This will aid the identification of the effective degrees of freedom underlying the resonance excitation of all states that couple to virtual photons.

VI. OTHER TOPICS IN LIGHT QUARK BARYON SPECTROSCOPY THAT ARE ADDRESSED WITH THIS LOI.

Besides the search for hybrid baryon states, there are many open issues in our knowledge of the structure of ordinary (non-gluonic) baryon excitations, that can be addressed with data coming from the same experiment that are taken in parallel. As an example we show in Fig. 18 the electrocouplings of the $N(1680)\frac{5}{2}^+$ resonance, the strongest state in the third nucleon resonance region. With the exception of the real photon point, the data are quite sparse for $Q^2 \leq 1.8\text{GeV}^2$ and the extremely high statistics data expected from this project could address many of such questions for other states as well. Note that the high Q^2 part will be covered by the approved JLab experiment E12-09-003.

An even more compelling example is the $N(1675)\frac{5}{2}^-$ state where data at $Q^2 > 1.8\text{GeV}^2$ have been published recently by the CLAS collaboration [15]. Figure 19 shows the currently available helicity amplitudes. The low Q^2 data are

very important as for this state any non-zero values of the electro-coupling amplitudes will measures the strength of the meson-baryon contributions as the quark transitions are strongly suppressed by the Moorhouse selection rule. The main data needed are single pion production $ep \to e'\pi^+ n$ and $ep \to e'\pi^0 p$. These processes can be accumulated with sufficiently high event rate even with a pre-scale factor of 10 or more should the overall event rate be too high in this 2-prong topology.

VII. BEAMTIME ESTIMATE

The complete hybrid baryon program will require 3 beam energies at 6.6 GeV, 8.8 GeV, and 11 GeV to cover with highest statistics the lowest Q^2 range where the scattered electron is detected in the angle range from $2.5 \leq \theta_e \leq 4.5$deg. For the proposal we will likely request new beam time of 60 days that is divided into 20 days at 6.6 GeV, and 40 days at 8.8 GeV. The 11 GeV data of 60 days will be taken simultaneously with the already approved experiment E12-11-005.

VIII. INCORPORATING HYBRID BARYON EXCITATIONS IN MONTE CARLO SIMULATION OF EXCLUSIVE KY ELECTROPRODUCTION.

The feasibility to observe hybrid-baryon will be explored in the Monte-Carlo simulation of KY electroproduction. The KY event distributions over the center-of-mass (CM) kaon emission angle θ_K will be simulated using two reaction models for KY electroproduction cross sections and accounting for the CLAS12 acceptance/efficiency :

- the coherent superposition of reggeized non-resonant amplitudes and the contribution from the established N* states [17, 29]. The web-site [30] provides the full set of observables of KY electroproduction off protons computed in the aforementioned approaches (the model A); and
- incorporating incoherently in addition to the model A the cross sections for KY production through electroexcitation of hybrid-baryon state in the virtual-photo-proton s-channel (the model B).

Confronting the event distributions over the CM angle of the final kaons simulated in the two aforementioned models, we can determine the minimal absolute values of the hybrid-baryon electroexcitation amplitudes above which the signal from hybrid state will be visible in the difference between event distributions simulated with/without the hybrid-baryon state.

According to the LQCD results [11] shown in Fig 1, there are two nearly degenerated states of ≈ 2.6 GeV masses with significant contributions from strongly coupled to glue quark configurations. These two states have spin-parities $J^\pi=1/2^+$ and $3/2^+$. Currently, the LQCD studies [11] were carried out with masses of light constituent quarks that are still far from their physical values. They give unphysical pion mass of ≈ 400 MeV. We need to correct the [11] prediction for the hybrid-baryon masses employing the mass shift towards smaller mass values which can be expected when quark and pion masses are approaching their physical values. For the hybrid state of $J^\pi=1/2^+$ such mass shift can be evaluated as the difference Δ_1 between the [11] results on the mass of the lightest nucleon of spin-parity $J^\pi=1/2^+$ and the measured value of the proton mass: $\Delta_1 \approx 0.04$ GeV. The mass shift for the hybrid-baryon of spin-parity $J^\pi=3/2^+$ can be evaluated as the difference Δ_2 between the mass of lightest resonance of $J^\pi=3/2^+$ from LQCD [11] and the measured mass of N(1720)$3/2^+$-resonance: $\Delta_2 \approx 0.05$ GeV.

Based on these simple estimates, we will implement hybrid-baryons of the two possible values of spin-parity $1/2^+$ and $3/2^+$ in the mass interval from 2.1 to 2.2 GeV in the simulation of the KY electroproduction cross section in the model B. According to the RPP14 results citeAgashe:2014kda on the total decay widths of nucleon resonances with masses ≈ 2.0 GeV and their branching fraction (BF) to the KY final states, we adopt for the total decay width of hybrid-baryon the range from 250 to 300 MeV and for its BF to the KY final states the value of 5 %.

The LQCD evaluations [11] (see Fig 1) also predict the particular pattern in the spectrum of hybrid states. In both partial waves with $J^\pi=1/2^+$ and $J^\pi=3/2^+$ the hybrid states of the minimal masses should be the excited nucleon states, while the next levels of the excited hybrid-baryons should be Δ^* resonances with masses close to the masses of the N^* hybrid states of minimal masses. This spectrum pattern being observed in the data may also support the signature of the hybrid-baryon states.

The cross sections for the contribution from the hybrid-baryon state can be evaluated from the resonant amplitudes according to the Eq. (44) in the Appendix A. A relativistic Breit-Wigner (BW) ansatz was used successfully for the parameterisation of the resonant amplitudes, allowing us to extract $\gamma_v NN^*$ electrocouplings from the CLAS data on exclusive charged double pion electroproduction off protons [26]. In the helicity representation $\langle \lambda_f \, | T_r | \, \lambda_\gamma \lambda_p \rangle$ resonant

amplitude for a single contributing resonance can be written as:

$$\langle \lambda_f \left| T_r \right| \lambda_\gamma \lambda_p \rangle = \frac{\langle \lambda_f \left| T_{dec} \right| \lambda_R \rangle \langle \lambda_R \left| T_{em} \right| \lambda_\gamma \lambda_p \rangle}{M_r^2 - W^2 - i\Gamma_r M_r}, \tag{2}$$

where M_r and Γ_r are the resonance mass and total width, respectively. For the particular purpose of the cross section evaluation for the EG we employ the energy independent total/partial resonance decay widths. Such parameterisation is not able to provide the proper amplitude behavior near threshold. In the amplitude analyses, the energy dependence of the resonance total and partial decay widths should be implemented, as described in [24]. The matrix elements $\langle \lambda_R \left| T_{em} \right| \lambda_\gamma \lambda_p \rangle$ and $\langle \lambda_f \left| T_{dec} \right| \lambda_R \rangle$ are the electromagnetic production and hadronic decay amplitudes of the N^* with helicity $\lambda_R = \lambda_\gamma - \lambda_p$, in which λ_γ and λ_p stand for the helicities of the photon and proton in the initial state, and λ_f represents the helicities of final-state hadrons in the N^* decays. The hadronic decay amplitudes $\langle \lambda_f | T_{dec} | \lambda_R \rangle$ are related to the Γ_{λ_f} partial hadronic decay widths of the N^* to KY final states f of helicity $\lambda_f = \lambda_Y$ by:

$$\langle \lambda_f | T_{dec} | \lambda_R \rangle = \langle \lambda_f | T^{J_r}_{dec} | \lambda_R \rangle d^{J_r}_{\mu\nu}(\cos\theta_K) e^{i\mu\phi_K},$$

with $\mu = \lambda_R$ and $\nu = -\lambda_Y$, and

$$\langle \lambda_f | T^{J_r}_{dec} | \lambda_R \rangle = \frac{2\sqrt{2\pi}\sqrt{2J_r+1} M_r \sqrt{\Gamma_{\lambda_f}}}{\sqrt{p_i^r}} \sqrt{\frac{p_i^r}{p_i}}. \tag{3}$$

The means p_i^r and p_i are the magnitudes of the three-momenta of the final K for the $N^* \to K\Lambda$ decay (i=1) or for the $N^* \to K\Sigma$ decay (i=2), evaluated at $W = M_r$ and at the running W, respectively. The variables θ_K, ϕ_K are the CM polar and azimuthal angles for the final kaon. The symbol J_r stands for the N^* spin.

The final Λ or Σ baryons can be only in the helicity states $\lambda_f = \pm\frac{1}{2}$. The hadronic decay amplitudes $\langle \lambda_f | T^{J_r}_{dec} | \lambda_R \rangle$ with $\lambda_f = \pm\frac{1}{2}$ are related by P-invariance, which imposes the equal absolute values for both amplitudes. Therefore, the hybrid state partial decay widths to the KΛ and KΣ final states Γ_{λ_f} can be estimated as:

$$\Gamma_{\lambda_f} = \frac{1}{2}\Gamma_r 0.05, \tag{4}$$

where the factor 0.05 reflects the adopted 5% BF for hybrid-baryon decays to the KY final state.

The resonance electroexcitation amplitudes $\langle \lambda_R \left| T_{em} \right| \lambda_\gamma \lambda_p \rangle$ in Eq. (13) are related to the $\gamma_v N N^*$ electrocouplings $A_{1/2}$, $A_{3/2}$, and $S_{1/2}$ for nucleons. The definition of these electrocouplings in the JM model [26], which we are using in the LOI, is consistent with the Review of Particle Physics (RPP) [1] relation between the $A_{1/2}$, $A_{3/2}$ electrocouplings and the N^* electromagnetic decay width Γ_γ:

$$\Gamma_\gamma = \frac{q^2_{\gamma,r}}{\pi} \frac{2M_N}{(2J_r+1)M_r} \left[\left| A_{1/2} \right|^2 + \left| A_{3/2} \right|^2 \right], \tag{5}$$

where $q_{\gamma,r}$ is the three-momentum modulus of the photon at $W = M_r$ in the CM frame. The transition amplitudes $\langle \lambda_R \left| T_{em} \right| \lambda_\gamma \lambda_p \rangle$ are related to the $\gamma_v N N^*$ $A_{1/2}$, $A_{3/2}$, and $S_{1/2}$ electrocouplings by imposing the requirement that the BW parameterisation [31] of the resonant cross section for a single contributing resonance should be reproduced:

$$\sigma(W) = \frac{\pi}{q^2_\gamma}(2J_r+1) \frac{M_r^2 \Gamma_i(W) \Gamma_\gamma}{(M_r^2 - W^2)^2 - M_r^2 \Gamma_r^2} \frac{q_\gamma}{K}. \tag{6}$$

Here the photon equivalent energy $K = \frac{W^2 - M_N^2}{2W}$, q_γ is the absolute value of the initial photon three-momentum of virtuality $Q^2 > 0$ $q_\gamma = \sqrt{Q^2 + E^2_\gamma}$ and the energy E_γ in the CM frame at the running W

$$E_\gamma = \frac{W^2 - Q^2 - M_N^2}{2W}. \tag{7}$$

The $q_{\gamma,r}$ value in Eq. (16) can be computed from Eq. (18) at W=M_r. Γ_i is the total decay width to the final state $K\Lambda$ (i=1) or $K\Sigma$ (i=2). The factor $\frac{q_\gamma}{K}$ in Eq. (17) is equal to unity at the photon point. It accounts for the choice [27] of the virtual photon flux in the evaluation of the virtual photon cross sections. In this way we obtain the following

relationship between the transition amplitudes $\langle \lambda_R \left| T_{em} \right| \lambda_\gamma \lambda_p \rangle$ and the $\gamma_v N N^*$ electrocouplings:

$$\langle \lambda_R \left| T_{em} \right| \lambda_\gamma \lambda_p \rangle = \frac{W}{M_r} \sqrt{\frac{8 M_N M_r q_{\gamma_r}}{4\pi\alpha}} \sqrt{\frac{q_{\gamma_r}}{q_\gamma}} A_{1/2,3/2}(Q^2), \tag{8}$$

$$\text{with } |\lambda_\gamma - \lambda_p| = \frac{1}{2}, \frac{3}{2} \text{ for transverse photons, and}$$

$$\langle \lambda_R \left| T_{em} \right| \lambda_\gamma \lambda_p \rangle = \frac{W}{M_r} \sqrt{\frac{16 M_N M_r q_{\gamma_r}}{4\pi\alpha}} \sqrt{\frac{q_{\gamma_r}}{q_\gamma}} S_{1/2}(Q^2),$$

$$\text{for longitudinal photons.}$$

The factor $4\pi\alpha$ in Eqs. (19) reflects the particular relationship between the JM model amplitudes and cross sections [24], when the absolute value of the electron charge is factorized out of the production amplitudes.

With the resonant amplitudes of Eq. (13) one-fold differential cross sections for KY electroproduction off protons by virtual photons can be computed according to Eq (44) in the Appendix A. They should be further converted to the three-fold measurable electroproduction cross sections employing Eq (27) of the Appendix A. Obtained in this way cross section that correspond to the contribution from hybrid baryon should be added to the cross sections of model A (without hybrid state) in order to obtain the cross sections of model B (with the contribution from hybrid state). The angular distributions for the selected KY events over the CM kaon emission angles should be simulated both in the model A and in the model B accounting for the CLAS12 acceptance/efficiency in each bin of W and Q^2 covered by the proposed experiment. The difference in angular distributions for selected KY events simulated in the models A and B provides information on possibility to observe manifestation of hybrid-baryon state.

In order to quantify the statistical significance of the difference between exclusive KY event distributions over the CM θ_K angle simulated in the models A and B, the following value of $\chi^2/d.p.$ will be used:

$$\chi^2/d.p. = \frac{1}{N_{d.p.}} \sum_{\theta_i, W_j} \frac{(N_{B_{i,j}} - N_{A_{i,j}})^2}{\delta_{i,j}^2}, \tag{9}$$

where $N_{A_{i,j}}$, $N_{B_{i,j}}$ are the numbers of KY events in the kinematics bin of θ_i and W_j simulated in the models A and B, respectively, taking into account the CLAS12 acceptance/efficiency, θ_i stands for the emission angle of kaon in the CM frame, the sum is running over all bins of W and θ_K in any given bin of Q^2. The $N_{d.p.}$ is the number of the data points in all bins of W and θ included to the sum Eq. (20) The values of $\chi^2/d.p.$ will be evaluated independently in each bin of Q^2. The CM K emission angles are running from zero to 180 deg. The sum over W covers the range from 1.9 GeV to 2.4 GeV, which is expected to be the most sensitive to the contributions from hybrid-baryons of the minimal masses. Assuming the contribution from the statistic uncertainties only, the uncertainties for the difference between the angular event distributions $N_{B_{i,j}}$-$N_{A_{i,j}}$, simulated in the models B and A, respectively, $\delta_{i,j}$ can be evaluated as:

$$\delta_{i,j} = \sqrt{N_{A_{i,j}} + N_{B_{i,j}}} \tag{10}$$

Inserting Eq. (21) into Eq. (20), we obtain the final expression for the $\chi^2/d.p.$:

$$\chi^2/d.p. = \frac{1}{N_{d.p.}} \sum_{\theta_i, W_j} \frac{(N_{B_{i,j}} - N_{A_{i,j}})^2}{N_{B_{i,j}} + N_{A_{i,j}}}, \tag{11}$$

The studies of the signals from the hybrid-baryons of spin-parities $1/2^+$ and $3/2^+$ will be carried out. Electroexcitation of the former state can be described by two $A_{1/2}$ and $S_{1/2}$ electrocouplings. The latter state should be described by three electrocouplings $A_{1/2}$, $S_{1/2}$, and $A_{3/2}$. The definitions of all electrocouplings can be found in the review [5]. The information on the expected Q^2-evolution of the aforementioned electrocouplings for hybrid states, up to our knowledge, is currently not available. The purpose of our studies will be: varying hybrid baryon electrocouplings to determine their minimal absolute values above which the signal from the hybrid baryon will be observed in the difference between the CM K-angular distributions estimated in the models A and B or without/with the hybrid-baryon. These studies will be done independently in each bin of Q^2 for the proposed experiment.

The following restrictions will be imposed in variation of the hybrid-baryon electrocouplings, assuming the positive values of all electrocouplings:

- **the hybrid-baryon of $3/2^+$-spin-parity:** Three electrocouplings $A_{1/2}$, $S_{1/2}$, and $A_{3/2}$ will be computed varying positive parameter A as:

$$\begin{aligned} A_{1/2} &= A, \\ S_{1/2} &= AQ, \\ A_{3/2} &= A/Q^2, \\ Q &= \sqrt{Q^2} \end{aligned} \tag{12}$$

  The relations Eq. (23) for the hybrid baryon electrocouplings are expected in the model studies [9] for manifestation of of the hybrid-baryon signature;

- **the hybrid-baryon of $1/2^+$-spin-parity:** $A_{1/2}$ electrocouplings will be varied assuming $S_{1/2}$=0 GeV$^{-1/2}$. Such behavior of $S_{1/2}$ was expected in the studies [14] of N(1440)$1/2^+$ resonance structure assuming that this state represent the hybrid baryon. In another simulation we will employ the relations Eq (23) with $A_{3/2}$=0 GeV$^{-1/2}$.

For several trial sets of hybrid state electrocouplings computed as described above we will simulate the event distributions over the CM K-emission angles in all bins of W and Q^2 covered by measurements in the models B with hybrid-baryon contribution and compare them with the model A without hybrid baryon in ech bin of Q^2 independently. The values of $\chi^2/d.p.$ evaluated according to the Eq. (22) will elucidate the feasibility for the hybrid-baryon observation. The $\chi^2/d.p.$ above 2. will be considered as the statisticaly significant signal from the hybrid-baryon. The minimal absolute values of hybrid-baryons electocouplings above which $\chi^2/d.p.$ becomes larger than 2 will be treated as the minimal values of hybrid electrocouplings above which the signal from hybrid-baryon can be observed in the proposed experiment.

The described above simulations will provide the information on minimal absolute values of hybrid-baryon electrocouplings as the functions of Q^2 above which the signal from the hybrid-baryon can be detected in the proposed experiment. They can be compared with the expected values of hybrid electrocouplings from any model.

IX. SUMMARY

In this letter we discussed an extensive program to study the excitation of nucleon resonances in meson electroproduction using electron beam of 6.6, 8.8, and 11 GeV energy. The main focus is on the search for gluonic excitations of light-quark baryons in the mass range up to 3.5 GeV, and in the range of Q^2 from 0.05 to 2.0 GeV^2. We have estimated the rates for two of the channels we propose to study, $K^+\Lambda$ ($K^+\Sigma$) and $p\pi^+\pi^-$, but all other channels detected in CLAS12 will be subjected to analyses as well. The expected rates are very high, thanks to the very forward scattered electrons with minimum $Q^2 = 0.05$GeV^2 that are detected in the Forward Tagger. The data will be subjected to state-of-the-art partial wave analyses that were developed during the past years for baryon resonance analyses. Beyond the main focus of the LOI on hybrid baryons, a wealth of data will be collected in many different channels that will put meson electroproduction data on par with real photo production in terms of production rates and allow for the vast extension of the ongoing N* electroexcitation program with CLAS at lower energies.

X. FUTURE MONTE-CARLO STUDIES FOR MANIFESTATION OF HYBRID BARYONS IN EXCLUSIVE KY ELECTROPRODUCTION.

The feasibility to observe hybrid-baryon will be explored in the Monte-Carlo simulation of KY electroproduction. The KY event distributions over the center-of-mass (CM) kaon emission angle θ_K will be simulated using two reaction models for KY electroproduction cross sections and accounting for the CLAS12 acceptance/efficiency :

- the coherent superposition of reggeized non-resonant amplitudes and the contribution from the established N* states [17, 29]. The web-site [30] provides the full set of observables of KY electroproduction off protons computed in the aforementioned approaches (the model A); and
- incorporating incoherently in addition to the model A the cross sections for KY production through electroexcitation of hybrid-baryon state in the virtual-photo-proton s-channel (the model B).

Confronting the event distributions over the CM angle of the final kaons simulated in the two aforementioned models, we can determine the minimal absolute values of the hybrid-baryon electroexcitation amplitudes above which the signal from hybrid state will be visible in the difference between event distributions simulated with/without the hybrid-baryon state.

According to the LQCD results [11] shown in Fig 1, there are two nearly degenerated states of ≈ 2.6 GeV masses with significant contributions from strongly coupled to glue quark configurations. These two states have spin-parities J^π=$1/2^+$ and $3/2^+$. Currently, the LQCD studies [11] were carried out with masses of light constituent quarks that are still far from their physical values. They give unphysical pion mass of ≈ 400 MeV. We need to correct the [11] prediction for the hybrid-baryon masses employing the mass shift towards smaller mass values which can be expected when quark and pion masses are approaching their physical values. For the hybrid state of J^π=$1/2^+$ such mass shift can be evaluated as the difference Δ_1 between the [11] results on the mass of the lightest nucleon of spin-parity J^π=$1/2^+$ and the measured value of the proton mass: $\Delta_1 \approx 0.04$ GeV. The mass shift for the hybrid-baryon of spin-parity J^π=$3/2^+$ can be evaluated as the difference Δ_2 between the mass of lightest resonance of J^π=$3/2^+$ from LQCD [11] and the measured mass of N(1720)$3/2^+$-resonance: $\Delta_2 \approx 0.05$ GeV.

Based on these simple estimates, we will implement hybrid-baryons of the two possible values of spin-parity $1/2^+$ and $3/2^+$ in the mass interval from 2.1 to 2.2 GeV in the simulation of the KY electroproduction cross section in the model B. According to the RPP14 results [1] on the total decay widths of nucleon resonances with masses ≈ 2.0 GeV and their branching fraction (BF) to the KY final states, we adopt for the total decay width of hybrid-baryon the range from 250 to 300 MeV and for its BF to the KY final states the value of 5 %.

The LQCD evaluations [11] (see Fig 1) also predict the particular pattern in the spectrum of hybrid states. In both partial waves with J^π=$1/2^+$ and J^π=$3/2^+$ the hybrid states of the minimal masses should be the excited nucleon states, while the next levels of the excited hybrid-baryons should be Δ^* resonances with masses close to the masses of the N^* hybrid states of minimal masses. This spectrum pattern being observed in the data may also support the signature of the hybrid-baryon states.

The cross sections for the contribution from the hybrid-baryon state can be evaluated from the resonant amplitudes according to the Eq. (44) in the Appendix A. A relativistic Breit-Wigner (BW) ansatz was used successfully for the parameterisation of the resonant amplitudes, allowing us to extract $\gamma_v NN^*$ electrocouplings from the CLAS data on exclusive charged double pion electroproduction off protons [26]. In the helicity representation $\langle \lambda_f \left| T_r \right| \lambda_\gamma \lambda_p \rangle$ resonant amplitude for a single contributing resonance can be written as:

$$\langle \lambda_f \left| T_r \right| \lambda_\gamma \lambda_p \rangle = \frac{\langle \lambda_f \left| T_{dec} \right| \lambda_R \rangle \langle \lambda_R \left| T_{em} \right| \lambda_\gamma \lambda_p \rangle}{M_r^2 - W^2 - i\Gamma_r M_r}, \tag{13}$$

where M_r and Γ_r are the resonance mass and total width, respectively. For the particular purpose of the cross section evaluation for the EG we employ the energy independent total/partial resonance decay widths. Such parameterisation is not able to provide the proper amplitude behavior near threshold. In the amplitude analyses, the energy dependence of the resonance total and partial decay widths should be implemented, as described in [24]. The matrix elements $\langle \lambda_R \left| T_{em} \right| \lambda_\gamma \lambda_p \rangle$ and $\langle \lambda_f \left| T_{dec} \right| \lambda_R \rangle$ are the electromagnetic production and hadronic decay amplitudes of the N^* with helicity $\lambda_R = \lambda_\gamma - \lambda_p$, in which λ_γ and λ_p stand for the helicities of the photon and proton in the initial state, and λ_f represents the helicities of final-state hadrons in the N^* decays. The hadronic decay amplitudes $\langle \lambda_f | T_{dec} | \lambda_R \rangle$ are related to the Γ_{λ_f} partial hadronic decay widths of the N^* to KY final states f of helicity $\lambda_f = \lambda_Y$ by:

$$\langle \lambda_f | T_{dec} | \lambda_R \rangle = \langle \lambda_f | T^{J_r}_{dec} | \lambda_R \rangle d^{J_r}_{\mu\nu}(\cos\theta_K) e^{i\mu\phi_K},$$

with $\mu = \lambda_R$ and $\nu = -\lambda_Y$, and

$$\langle \lambda_f | T^{J_r}_{dec} | \lambda_R \rangle = \frac{2\sqrt{2\pi}\sqrt{2J_r+1} M_r \sqrt{\Gamma_{\lambda_f}}}{\sqrt{p_i^r}} \sqrt{\frac{p_i^r}{p_i}}. \tag{14}$$

The means p_i^r and p_i are the magnitudes of the three-momenta of the final K for the $N^* \to K\Lambda$ decay (i=1) or for the $N^* \to K\Sigma$ decay (i=2), evaluated at $W = M_r$ and at the running W, respectively. The variables θ_K, ϕ_K are the CM polar and azimuthal angles for the final kaon. The symbol J_r stands for the N^* spin.

The final Λ or Σ baryons can be only in the helicity states $\lambda_f = \pm\frac{1}{2}$. The hadronic decay amplitudes $\langle\lambda_f|T_{dec}^{J_r}|\lambda_R\rangle$ with $\lambda_f = \pm\frac{1}{2}$ are related by P-invariance, which imposes the equal absolute values for both amplitudes. Therefore, the hybrid state partial decay widths to the KΛ and KΣ final states Γ_{λ_f} can be estimated as:

$$\Gamma_{\lambda_f} = \frac{1}{2}\Gamma_r 0.05, \tag{15}$$

where the factor 0.05 reflects the adopted 5% BF for hybrid-baryon decays to the KY final state.

The resonance electroexcitation amplitudes $\langle\lambda_R\,|T_{em}|\,\lambda_\gamma\lambda_p\rangle$ in Eq. (13) are related to the $\gamma_v NN^*$ electrocouplings $A_{1/2}$, $A_{3/2}$, and $S_{1/2}$ for nucleons. The definition of these electrocouplings in the JM model [26], which we are using in the LOI, is consistent with the Review of Particle Physics (RPP) [1] relation between the $A_{1/2}$, $A_{3/2}$ electrocouplings and the N^* electromagnetic decay width Γ_γ:

$$\Gamma_\gamma = \frac{q_{\gamma,r}^2}{\pi}\frac{2M_N}{(2J_r+1)M_r}\left[\left|A_{1/2}\right|^2 + \left|A_{3/2}\right|^2\right], \tag{16}$$

where $q_{\gamma,r}$ is the three-momentum modulus of the photon at $W = M_r$ in the CM frame. The transition amplitudes $\langle\lambda_R\,|T_{em}|\,\lambda_\gamma\lambda_p\rangle$ are related to the $\gamma_v NN^*$ $A_{1/2}$, $A_{3/2}$, and $S_{1/2}$ electrocouplings by imposing the requirement that the BW parameterisation [31] of the resonant cross section for a single contributing resonance should be reproduced:

$$\sigma(W) = \frac{\pi}{q_\gamma^2}(2J_r+1)\frac{M_r^2\Gamma_i(W)\Gamma_\gamma}{(M_r^2-W^2)^2 - M_r^2\Gamma_r^2}\frac{q_\gamma}{K}. \tag{17}$$

Here the photon equivalent energy $K = \frac{W^2-M_N^2}{2W}$, q_γ is the absolute value of the initial photon three-momentum of virtuality $Q^2 > 0$ $q_\gamma = \sqrt{Q^2+E_\gamma^2}$ and the energy E_γ in the CM frame at the running W

$$E_\gamma = \frac{W^2-Q^2-M_N^2}{2W}. \tag{18}$$

The $q_{\gamma,r}$ value in Eq. (16) can be computed from Eq. (18) at W=M_r. Γ_i is the total decay width to the final state $K\Lambda$ (i=1) or $K\Sigma$ (i=2). The factor $\frac{q_\gamma}{K}$ in Eq. (17) is equal to unity at the photon point. It accounts for the choice [27] of the virtual photon flux in the evaluation of the virtual photon cross sections. In this way we obtain the following relationship between the transition amplitudes $\langle\lambda_R\,|T_{em}|\,\lambda_\gamma\lambda_p\rangle$ and the $\gamma_v NN^*$ electrocouplings:

$$\langle\lambda_R\,|T_{em}|\,\lambda_\gamma\lambda_p\rangle = \frac{W}{M_r}\sqrt{\frac{8M_N M_r q_{\gamma_r}}{4\pi\alpha}}\sqrt{\frac{q_{\gamma_r}}{q_\gamma}}A_{1/2,3/2}(Q^2), \tag{19}$$

$$\text{with}\,|\lambda_\gamma - \lambda_p| = \frac{1}{2},\,\frac{3}{2}\quad\text{for transverse photons, and}$$

$$\langle\lambda_R\,|T_{em}|\,\lambda_\gamma\lambda_p\rangle = \frac{W}{M_r}\sqrt{\frac{16M_N M_r q_{\gamma_r}}{4\pi\alpha}}\sqrt{\frac{q_{\gamma_r}}{q_\gamma}}\,S_{1/2}(Q^2),$$

$$\text{for longitudinal photons.}$$

The factor $4\pi\alpha$ in Eqs. (19) reflects the particular relationship between the JM model amplitudes and cross sections [24], when the absolute value of the electron charge is factorized out of the production amplitudes.

With the resonant amplitudes of Eq. (13) one-fold differential cross sections for KY electroproduction off protons by virtual photons can be computed according to Eq (44) in the Appendix A. They should be further converted to the three-fold measurable electroproduction cross sections employing Eq (27) of the Appendix A. Obtained in this way cross section that correspond to the contribution from hybrid baryon should be added to the cross sections of model A (without hybrid state) in order to obtain the cross sections of model B (with the contribution from hybrid state). The angular distributions for the selected KY events over the CM kaon emission angles should be simulated both in the model A and in the model B accounting for the CLAS12 acceptance/efficiency in each bin of W and Q^2 covered by the proposed experiment. The difference in angular distributions for selected KY events simulated in the models A and B provides information on possibility to observe manifestation of hybrid-baryon state.

In order to quantify the statistical significance of the difference between exclusive KY event distributions over the CM θ_K angle simulated in the models A and B, the following value of $\chi^2/d.p.$ will be used:

$$\chi^2/d.p. = \frac{1}{N_{d.p.}} \sum_{\theta_i, W_j} \frac{(N_{B_{i,j}} - N_{A_{i,j}})^2}{\delta_{i,j}^2}, \tag{20}$$

where $N_{A_{i,j}}$, $N_{B_{i,j}}$ are the numbers of KY events in the kinematics bin of θ_i and W_j simulated in the models A and B, respectively, taking into account the CLAS12 acceptance/efficiency, θ_i stands for the emission angle of kaon in the CM frame, the sum is running over all bins of W and θ_K in any given bin of Q^2. The $N_{d.p.}$ is the number of the data points in all bins of W and θ included to the sum Eq. (20) The values of $\chi^2/d.p.$ will be evaluated independently in each bin of Q^2. The CM K emission angles are running from zero to 180 deg. The sum over W covers the range from 1.9 GeV to 2.4 GeV, which is expected to be the most sensitive to the contributions from hybrid-baryons of the minimal masses. Assuming the contribution from the statistic uncertainties only, the uncertainties for the difference between the angular event distributions $N_{B_{i,j}}$-$N_{A_{i,j}}$, simulated in the models B and A, respectively, $\delta_{i,j}$ can be evaluated as:

$$\delta_{i,j} = \sqrt{N_{A_{i,j}} + N_{B_{i,j}}} \tag{21}$$

Inserting Eq. (21) into Eq. (20), we obtain the final expression for the $\chi^2/d.p.$:

$$\chi^2/d.p. = \frac{1}{N_{d.p.}} \sum_{\theta_i, W_j} \frac{(N_{B_{i,j}} - N_{A_{i,j}})^2}{N_{B_{i,j}} + N_{A_{i,j}}}, \tag{22}$$

The studies of the signals from the hybrid-baryons of spin-parities $1/2^+$ and $3/2^+$ will be carried out. Electroexcitation of the former state can be described by two $A_{1/2}$ and $S_{1/2}$ electrocouplings. The latter state should be described by three electrocouplings $A_{1/2}$, $S_{1/2}$, and $A_{3/2}$. The definitions of all electrocouplings can be found in the review [5]. The information on the expected Q^2-evolution of the aforementioned electrocouplings for hybrid states, up to our knowledge, is currently not available. The purpose of our studies will be: varying hybrid baryon electrocouplings to determine their minimal absolute values above which the signal from the hybrid baryon will be observed in the difference between the CM K-angular distributions estimated in the models A and B or without/with the hybrid-baryon. These studies will be done independently in each bin of Q^2 for the proposed experiment.

The following restrictions will be imposed in variation of the hybrid-baryon electrocouplings, assuming the positive values of all electrocouplings:

- **the hybrid-baryon of $3/2^+$-spin-parity:** Three electrocouplings $A_{1/2}$, $S_{1/2}$, and $A_{3/2}$ will be computed varying positive parameter A as:

$$\begin{aligned} A_{1/2} &= A, \\ S_{1/2} &= AQ, \\ A_{3/2} &= A/Q^2, \\ Q &= \sqrt{Q^2} \end{aligned} \tag{23}$$

  The relations Eq. (23) for the hybrid baryon electrocouplings are expected in the model studies [9] for manifestation of of the hybrid-baryon signature;

- **the hybrid-baryon of $1/2^+$-spin-parity:** $A_{1/2}$ electrocouplings will be varied assuming $S_{1/2}$=0 GeV$^{-1/2}$. Such behavior of $S_{1/2}$ was expected in the studies [14] of N(1440)$1/2^+$ resonance structure assuming that this state represent the hybrid baryon. In another simulation we will employ the relations Eq (23) with $A_{3/2}$=0 GeV$^{-1/2}$.

For several trial sets of hybrid state electrocouplings computed as described above we will simulate the event distributions over the CM K-emission angles in all bins of W and Q^2 covered by measurements in the models B with hybrid-baryon contribution and compare them with the model A without hybrid baryon in each bin of Q^2 independently. The values of $\chi^2/d.p.$ evaluated according to the Eq. (22) will elucidate the feasibility for the hybrid-baryon observation. The $\chi^2/d.p.$ above 2. will be considered as the statisticaly significant signal from the hybrid-baryon. The minimal absolute values of hybrid-baryons electocouplings above which $\chi^2/d.p.$ becomes larger than 2 will be treated as the minimal values of hybrid electrocouplings above which the signal from hybrid-baryon can be observed in the proposed experiment.

The described above simulations will provide the information on minimal absolute values of hybrid-baryon electrocouplings as the functions of Q^2 above which the signal from the hybrid-baryon can be detected in the proposed experiment. They can be compared with the expected values of hybrid electrocouplings from any model.

XI. APPENDIX A.

All amplitudes were calculated for the S-matrix defined as:

$$S = I + (2\pi)^4 \delta^4(P_f - P_i) iT, \tag{24}$$

where P_f and P_i are total four momenta of the final and the initial particles respectively. The Dirac spinors were normalized as:

$$\overline{U_p} U_p = 2M_N, \tag{25}$$

where U_p, ($\overline{U_p}$) are Dirac (conjugated Dirac) spinors, M_N is the nucleon mass. With this parameterization of the S-matrix and Dirac spinor normalization, the phase space element for the final particle i with three-momentum vector $\vec{p_i}$ and energy E_i is defined as:

$$d^3\vec{p_i}/(2E_i(2\pi)^3), \tag{26}$$

All time-space tensors (currents, the particle four-momenta) correspond to the $g_{\mu\nu}$ tensor (μ=0,1,2,3) with the components: $g_{00} = 1$, $g_{11} = g_{22} = g_{33} = -1$.

The exclusive reactions cross-sections by virtual photons absorption off the protons were determined in the single photon exchange approximation. These cross-sections are related to the measured exclusive electron scattering cross-sections according to:

$$\frac{d^4\sigma}{dW dQ^2 d\Omega_K} = \Gamma_v \frac{d^2\sigma}{d\Omega_K} \tag{27}$$

where ν is virtual photon energy in the lab. frame, Γ_v is the virtual photon flux defined by the momenta of incoming and outgoing electrons:

$$\Gamma_v = \frac{\alpha}{4\pi} \frac{1}{E_b^2 M_p^2} \frac{W(W^2 - M_p^2)}{(1-\varepsilon)Q^2} \ , \tag{28}$$

and α is the fine structure constant, E_b is the beam energy, M_p is the proton mass, and ε is the virtual photon transverse polarization given by

$$\varepsilon = \left(1 + 2\left(1 + \frac{\nu^2}{Q^2}\right)\tan^2\left(\frac{\theta_e}{2}\right)\right)^{-1} \ , \tag{29}$$

where ν is the virtual photon energy and θ_e is the electron scattering angle in the laboratory frame. This formalism is described in details in [32]. $d\Omega_K$ stand for the element of the solid angle of kaon emission in the CM frame.

Alternatively, the exclusive cross sections in electron scattering off protons $\frac{d^5\sigma}{dE' d\Omega_{e'} d\Omega_K}$ can be obtained employing another set of variables for the scattered electron, where dE' and $d\Omega_{e'}$ represent differentials for energy and solid angle of the scattered electron in the Lab. frame. For this case, the Eq. (28) for the virtual photon flux should be modified as:

$$\Gamma_v^{'} = \frac{\alpha}{2\pi^2} \frac{E_{e'}}{E_b} \frac{W(W^2 - M_p^2)}{(1-\varepsilon)2M_p^2 Q^2} \ , \tag{30}$$

The Eq. (29) that determined polarisation of virtual photon remains unchanged.

The two-fold differential cross-section $\frac{d^2\sigma}{d\Omega_K}$ for KY production by virtual photons off the protons was calculated as a contraction of leptonic and hadronic tensors divided by the invariant virtual photon flux and multiplied by the phase space differential for the 2-body final state $d^2\Phi$:

$$d^2\Phi = \frac{q_K d\Omega_K}{4\pi^2 4W}, \tag{31}$$

where q_K is the kaon three momentum absolute value in the CM frame The leptonic tensor $L_{\mu\nu}$ is well known from QED [32]:

$$L_{\mu\nu} = 2p_{\mu_{e_i}} p_{\nu_{e_f}} - 2p_{\nu_{e_i}} p_{\mu_{e_f}} - g_{\mu\nu} Q^2, \tag{32}$$

The hadronic tensor $W_{\mu\nu}$ represents a product of the hadronic currents J^*_μ and J_ν contracted to the spin-density matrices for the initial and the final hadrons:

$$W_{\mu\nu} = \sum_{\lambda_{p'},\lambda_p,\lambda_{f'},\lambda_f} J^*_\mu(\lambda_{p'},\lambda_{f'}) J_\nu(\lambda_p,\lambda_f) \rho_{\lambda_{p'},\lambda_p} \rho_{\lambda_{f'},\lambda_f}, \tag{33}$$

where $\lambda_{p'}$,λ_p stand for the helicities of the initial proton, while $\lambda_{f'}$, λ_f stand for the helicities of the final hadrons, $\rho_{\lambda_{p'},\lambda_p}$, $\rho_{\lambda_{f'},\lambda_f}$ are the density matrices for the initial protons and final hadrons. In a case of unplolarized the initial proton and the final hadrons, they have the simplest representation:

$$\begin{aligned} \rho_{\lambda_{p'},\lambda_p} &= \frac{1}{2} I \\ \rho_{\lambda_{f'},\lambda_f} &= I. \end{aligned} \tag{34}$$

Contrating the leptonic Eq. (32) and hadronic Eq. (33) tensors in the lab. frame we obtain the following expression for one-fold differential KY cross section by virtual photons absorption off the protons $\frac{d\sigma}{d(-cos(\theta_K))}$:

$$\begin{aligned} \frac{d\sigma}{d\Omega_K} = \frac{4\pi\alpha}{4K_L M_N} [\frac{J^*_x J_x + J^*_y J_y}{2} + \epsilon_L J^*_z J_z \\ + \epsilon_T \frac{J^*_x J_x - J^*_y J_y}{2} + \sqrt{2\epsilon_L(1+\epsilon_T)} \frac{J^*_x J_z + J^*_z J_x}{2}] \frac{q_K}{4\pi^2 4W}, \end{aligned} \tag{35}$$

where α is fine structure constant, ϵ_L stands for degree of longitudinal polarization of virtual photons. The QED calculations give for ϵ_L[32]:

$$\epsilon_L = \sqrt{\frac{Q^2}{\nu^2}} \epsilon. \tag{36}$$

The factor $4K_L M_N$ is the invariant virtual photon flux, M_N is nucleon mass, K_L is the equivalent photon energy:

$$K_L = \frac{W^2 - M_N^2}{2M_N}, \tag{37}$$

Four terms in Eq. (35) generate four structure functions that determine $\frac{d\sigma}{d\Omega_K}$ exclusive electroproduction cross section -transverse (T), longitudinal (L) and two interference structure functions transverse-transverse (TT) and transverse-longitudinal (TL):

$$\frac{d\sigma}{d\Omega_K} = \frac{d\sigma_T}{d\Omega_K} + \epsilon_L \frac{d\sigma_L}{d\Omega_K} + \epsilon_T \frac{d\sigma_{TT}}{d(\Omega_K} cos(2\phi_K) + \sqrt{2\epsilon_L(1+\epsilon_T)} \frac{d\sigma_{TL}}{d(\Omega_K} cos(\phi_K) \tag{38}$$

The ϕ_K dependence for $\frac{d\sigma}{d\Omega_K}$ cross section is imposed by rotational invariance of the electroproduction amplitudes, therefore. it is a model independent.

This LOI deals with spin averaged differential cross sections, that are independent from any polarization observable. In order to get rid of virtual photon polarization degree of freedom, we integrate $d^2\sigma/d\Omega_K$ cross-section for KY production by virtual photons Eqs. (35, 38) , as well as $d^2\Phi$ phase space in Eq. (31), over the azimuthal ϕ_K angle of of the final kaon. After that the Eqs. (35, 38) are reduced to the simpler expressions

$$\frac{d\sigma}{d(-cos(\theta_K))} = \frac{4\pi\alpha}{4K_L M_N} \left\{ \frac{J^*_x J_x + J^*_y J_y}{2} + \epsilon_L J^*_z J_z \right\} \frac{q_K}{2\pi 4W}, \tag{39}$$

$$\frac{d\sigma}{d\Omega_K} = \frac{d\sigma_T}{d\Omega_K} + \epsilon_L \frac{d\sigma_L}{d\Omega_K} \tag{40}$$

Only ϕ_K independent structure functions remain non-zero after integration over ϕ_K angle.

The hadronic current J_ν and the virtual photon vectors $\epsilon(\lambda_\gamma)$ (λ_γ=-1,0,+1) are related to reaction helicity amplitudes $\langle \lambda_f | T | \lambda_p \lambda_\gamma \rangle$ as:

$$\begin{aligned} \epsilon_\nu(\lambda_\gamma = -1) J^\nu(\lambda_p,\lambda_f) = \langle \lambda_f | T | \lambda_p \lambda_\gamma = -1 \rangle, \\ \epsilon_\nu(\lambda_\gamma = 1) J^\nu(\lambda_p,\lambda_f) = \langle \lambda_f | T | \lambda_p \lambda_\gamma = 1 \rangle, \\ \epsilon_\nu(\lambda_\gamma = 0) J^\nu(\lambda_p,\lambda_f) = \langle \lambda_f | T | \lambda_p \lambda_\gamma = 0 \rangle, \end{aligned} \tag{41}$$

whereλ_i (i=γ, p) stand for the initial state photon and proton helicities. The λ_f is generic symbol for the helicities in the final state. The vectors $\epsilon(\lambda_\gamma)$ were estimated in the lab. frame, resulting in the hadronic currents and hadronic tensor determined in lab. frame. Contracted components of the leptonic and the hadronic tensors should be determined in the same frame. Therefore, components of the leptonic tensor should calculated in the lab. frame. This is a reason why the kinematical variables in Eqs. (29), (36) were evaluated in the lab. frame.

The J_0 component of the hadronic current was obtained employing current conservation:

$$q_0 J^0 - q_z J^z = 0. \tag{42}$$

The hadronic currents J_ν were derived from Eqs. (41-42):

$$\begin{aligned} J_x &= -\frac{\langle\lambda_f|T|\lambda_p\lambda_\gamma=1\rangle - \langle\lambda_f|T|\lambda_p\lambda_\gamma=-1\rangle}{\sqrt{2}}, \\ J_y &= i\frac{\langle\lambda_f|T|\lambda_p\lambda_\gamma=1\rangle + \langle\lambda_f|T^|\lambda_p\lambda_\gamma=-1\rangle}{\sqrt{2}}, \\ J_z &= \frac{\nu}{\sqrt{Q^2}}\langle\lambda_f|T|\lambda_p\lambda_\gamma=0\rangle. \end{aligned} \tag{43}$$

Inserting the single resonance production amplitudes Eqs.(13) and (14) to the currents determined by Eq. (43) , we obtain the final expressions for the transverse $\frac{d\sigma_T}{d(-cos(\theta_K))}$ and the longitudinal $\frac{d\sigma_L}{d(-cos(\theta_K))}$ cross section for KY electroproduction by virtual photons off unpolarized protons from the Eq. (39) with density matrices for the initial and the final states determined by Eq. (34) :

$$\begin{aligned} \frac{d\sigma_T}{d(-cos(\theta_K))} &= \frac{4\pi\alpha}{4K_L M_N}\frac{1}{2}\frac{1}{2}\sum_{\lambda_\gamma=\pm1,\lambda_p,\lambda_f}\frac{\langle\lambda_R\,|T_{em}|\,\lambda_\gamma\lambda_p\rangle^2\langle\lambda_f|T^{J_r}_{dec}|\lambda_R\rangle^2 d^{J_r^2}_{\mu\nu}(\cos\theta_K)}{(M_r^2-W^2)^2+(\Gamma_r M_r)^2}\frac{q_K}{2\pi 4W}, \\ \frac{d\sigma_L}{d(-cos(\theta_K))} &= \frac{4\pi\alpha}{4K_L M_N}\frac{1}{2}\sum_{\lambda_\gamma=0,\lambda_p,\lambda_f}\frac{\langle\lambda_R\,|T_{em}|\,\lambda_\gamma\lambda_p\rangle^2\langle\lambda_f|T^{J_r}_{dec}|\lambda_R\rangle^2 d^{J_r^2}_{\mu\nu}(\cos\theta_K)}{(M_r^2-W^2)^2+(\Gamma_r M_r)^2}\frac{q_K}{2\pi 4W}, \\ \mu &= \lambda\gamma - \lambda_p. \\ \nu &= -\lambda_Y, \end{aligned} \tag{44}$$

Resonance electroproduction $\langle\lambda_R\,|T_{em}|\,\lambda_\gamma\lambda_p\rangle$ and hadronic decay $\langle\lambda_f|T^{J_r}_{dec}|\lambda_R\rangle$ amplitudes are determined by Eqs. (19) and (14), respectively.

Assuming uniform distribution of cross section from extra-resonance over ϕ_K-angle, differential cross sections $\frac{d\sigma}{d\Omega_K}$ can be computed as

$$\frac{d\sigma}{d\Omega_K} = \frac{1}{2\pi}[\frac{d\sigma_T}{d(-cos(\theta_K))} + \epsilon_L\frac{d\sigma_L}{d(-cos(\theta_K))}] \tag{45}$$

Differential cross section computed according to Eq. (44,45) should be added incoherently to the model [17, 29, 30] differential cross sections in order to obtain differential cross sections for KY production by virtual photons in the model B which accounts for the contribution from the hybrid baryon. These cross sections should be converted employing Eq. (27) to the measurable KY electroproduction cross sections, which should be used in the EG.

---

[1] explicit expressions for the photon vectors $\epsilon_\nu(\lambda_\gamma)$ may be found in [32].

[1] K. A. Olive *et al.* [Particle Data Group Collaboration], Chin. Phys. C **38**, 090001 (2014)
[2] I. G. Aznauryan *et al.* [CLAS Collaboration], Phys. Rev. C **78**, 045209 (2008).
[3] T. Barnes and F. E. Close, Phys. Lett. B **123**, 89 (1983); E. Golowich, E. Haqq, and G. Karl, Phys. Rev. D **28**, 160 (1983); C.E. Carlson and T.H. Hansson, Phys. Lett. B **128**, 95 (1983); I. Duck and E. Umland, Phys. Lett. B **128** (1983) 221.
[4] I. G. Aznauryan *et al.* [CLAS Collaboration], Phys. Rev. C **80**, 055203 (2009).
[5] I. G. Aznauryan and V. D. Burkert, Prog. Part. Nucl. Phys. **67**, 1 (2012).
[6] S. Capstick and P. R. Page, Phys. Rev. C **66**, 065204 (2002), [nucl-th/9904041]; Phys. Rev. D **60**, 111501 (1999), [nucl-th/0207027].
[7] P. R. Page, Int. J. Mod. Phys. A **20**, 1791 (2005).
[8] C. K. Chow, D. Pirjol and T. M. Yan, Phys. Rev. D **59**, 056002 (1999).
[9] C. E. Carlson and N. C. Mukhopadhyay, Phys. Rev. Lett. **67**, 3745 (1991).
[10] T. T. Takahashi and H. Suganuma, Phys. Rev. Lett. **90**, 182001 (2003).
[11] J. J. Dudek and R. G. Edwards, Phys. Rev. D **85**, 054016 (2012).
[12] N. Suzuki, B. Julia-Diaz, H. Kamano, T.-S. H. Lee, A. Matsuyama and T. Sato, Phys. Rev. Lett. **104**, 042302 (2010).
[13] Z. P. Li, Phys. Rev. D **44**, 2841 (1991).
[14] Z. P. Li, V. Burkert and Z. J. Li, Phys. Rev. D **46**, 70 (1992).
[15] K. Park *et al.* [CLAS Collaboration].
[16] T. Corthals, D. G. Ireland, T. Van Cauteren and J. Ryckebusch, Phys. Rev. C **75**, 045204 (2007).
[17] L. De Cruz, J. Ryckebusch, T. Vrancx and P. Vancraeyveld, Phys. Rev. C **86**, 015212 (2012).
[18] A. Afanasev, I. Akushevich, V. Burkert and K. Joo, Phys. Rev. D **66**, 074004 (2002).
[19] T. Corthals et al., Phys. Rev. C73, 045207 (2006)
[20] C.W. Akerlof et al., Phys. Rev. 163, 1482 (1967)
[21] M. Ripani, V. Mokeev, M. Anghinolfi, M. Battaglieri, G. Fedotov, E. Golovach, B. Ishkhanov and M. Osipenko *et al.*, Nucl. Phys. A **672**, 220 (2000).
[22] I. G. Aznauryan, V. D. Burkert, G. V. Fedotov, B. S. Ishkhanov and V. I. Mokeev, Phys. Rev. C **72**, 045201 (2005).
[23] V. I. Mokeev et al., in "Proc. of the Workshop on the Physics of Excited Nucleon. NSTAR2005", ed. by S. Capstick, V. Crede, P. Eugenio, World Scientific Publishing Co., p. 47.
[24] V. I. Mokeev, V. D. Burkert, T. S. H. Lee, L. Elouadrhiri, G. V. Fedotov and B. S. Ishkhanov, Phys. Rev. C **80**, 045212 (2009).
[25] M. Ripani *et al.* [CLAS Collaboration], Phys. Rev. Lett. **91**, 022002 (2003)
[26] V. I. Mokeev *et al.* [CLAS Collaboration], Phys. Rev. C **86**, 035203 (2012)
[27] G. V. Fedotov *et al.* [CLAS Collaboration], Phys. Rev. C **79**, 015204 (2009)
[28] E. Golovach et al., $\gamma p \to p\pi^+\pi^-$ cross sections from g11a experiment, CLAS ANALYSIS NOTE (in preparation).
[29] T. Vranx, J. Ryckebusch, and J. Nys, Phys. Rev. C**89**, 065202 (2014).
[30] The StrangeCalc web-site http://rprmodel.ugent.be/calc/
[31] D. Luke and P. Soding, Multiple Pion Photoproduction in the s Channel Resonance Region, Springer Tracts in Modern Physics 59 (1971).
[32] E. Amaldi, S. Fubini and G. Furlan, Pion Electroproduction. Springer Tracts in Modern Physics **83**, ed. by G.Hohler (Springer Verlag, Berlin 1979).